

AN EXAMINATION OF SURFACE DISPLACEMENT AT THE PORTUGUESE BEND
LANDSLIDE, SOUTHERN CALIFORNIA, USING RADAR INTERFEROMETRY

by

MAX DAVID CALABRO

A THESIS

Presented to the Department of Geological Sciences
and the Graduate School of the University of Oregon
in partial fulfillment of the requirements
for the degree of
Master of Science

September 2008

“An Examination of Surface Displacement at the Portuguese Bend Landslide, Southern California, Using Radar Interferometry,” a thesis prepared by Max David Calabro in partial fulfillment of the requirements for the Master of Science degree in the Department of Geological Sciences. This thesis has been approved and accepted by:

Dr. Joshua R. Roering, Chair of the Examining Committee

2-Sep-2008

Date

Committee in Charge: Dr. Joshua R. Roering, Chair
 Dr. David A. Schmidt
 Dr. Alan W. Rempel

Accepted by:

Dean of the Graduate School

SAR data constrain deformation of the Portuguese Bend landslide in space and time, and its movement is found to correlate with seasonal rainfall. Traditional InSAR methods estimate an average downslope displacement rate of 1.01 ± 0.44 m/yr during the summer months. Interferograms show a consistent loss in phase coherence over the landslide for epochs greater than six months, especially in the winter. Interferograms become incoherent as a result of large displacement, and incoherence is used to map the spatial extent of the slide through time. The displacement rate increases several weeks after the beginning of the rainy season as rainwater percolating into the slide elevates pore pressure. SAR data processed using the permanent scatterer technique are partially successful on the rapidly moving landslide. Scatterers are identified on the landslide, but rates are underpredicted due to unwrapping uncertainty. A model based on rainfall-initiated landslides constrains diffusivity using InSAR observations.

CURRICULUM VITAE

NAME OF AUTHOR: Max David Calabro

PLACE OF BIRTH: Bennington, VT

DATE OF BIRTH: August 17, 1984

GRADUATE AND UNDERGRADUATE SCHOOLS ATTENDED:

University of Oregon, Eugene
Amherst College

DEGREES AWARDED:

Master of Science in Geology, 2008, University of Oregon
Bachelor of Arts in Physics, 2006, Amherst College

AREAS OF SPECIAL INTEREST:

Remote Sensing
Geomorphology

PROFESSIONAL EXPERIENCE

Graduate Teaching Fellow, Department of Geological Sciences, University of
Oregon, Eugene, Oregon, 2006-2008

Teaching and Research Assistant, Department of Physics, Amherst College,
Amherst, Massachusetts, 2003-2006

PUBLICATIONS

Calabro, M., D. Schmidt, J. Roering, & R. Douglas (2007). Spatial and Temporal Characterization of the Portuguese Bend Landslide, California, Using InSAR. *Eos Transactions AGU*, 88 (52): G53A-07.

ACKNOWLEDGMENTS

I give my most sincere thanks to Professor David Schmidt for his valuable support in the preparation of this manuscript and for his generosity and insight throughout the research process. Special thanks to my thesis committee chair Professor Joshua Roering for his contributions, especially concerning landslide dynamics. Thanks also to my committee member Professor Alan Rempel for his comments and assistance with modeling, to Craig Thornley for his computing aid, and to Professor Robert Douglas of University of Southern California for supplying GPS data. Synthetic aperture radar data was provided by the European Space Agency through their North American distributors, Eurimage and SpotImage. Data were purchased by the WInSAR consortium with funding from NASA, USGS, and NSF.

TABLE OF CONTENTS

Chapter	Page
I. INTRODUCTION AND BACKGROUND	1
Project Motivation	1
Study Area and Geologic Setting	2
History of Landslides and Mitigation Attempts	4
Properties of the Portuguese Bend Landslide	6
Thesis Overview	7
II. REVIEW OF PREVIOUS WORK ON THE PBL AND INSAR TECHNIQUES	9
Overview	9
Previous Work on the Portuguese Bend	9
Satellite Interferometry	11
Using InSAR to Monitor Landslides	13
III. ANALYSIS OF INSAR DATA FOR THE PALOS VERDES PENINSULA	15
Overview	15
Interferogram Formation	15
Atmospheric Artifacts	17
Stacking Interferometric Pairs	19
Quantifying Interferogram Decorrelation	23
Temporal Mapping of Interferogram Decorrelation	25
Permanent Scatterers Method	30
IV. INTERPRETATION AND DISCUSSION OF INSAR RESULTS	37
Overview	37
Examining the Summer Interferogram Stack	37
Temporal Constraints on Decorrelation	41
The Effect of Rainfall on Decorrelation Level	43
Modeling for Hydraulic Diffusivity	46

Chapter	Page
V. SUMMARY AND CONCLUSIONS	52
APPENDICES	
A. TABLE OF SAR SCENES USED	56
B. SCENE INDEX FOR PS SERIES	59
REFERENCES	61

LIST OF FIGURES

Figure	Page
1. Study Area: The Palos Verdes Peninsula	2
2. Study Area: The Portuguese Bend Landslide	3
3. ERS Satellite Tracks	16
4. Removing Atmospheric Artifacts	18
5. 08/09/1997 - 09/13/1997 Interferogram	20
6. Stack of 12 Summer Interferograms for Track 170	22
7. Stack of 8 Summer Interferograms for Track 442	22
8. 12/23/1995 - 01/27/1996 Interferogram	26
9. 05/16/1998 - 06/05/1999 Interferogram	26
10. Decorrelation Level Mapped at the PBL	28
11. Full Time Series of Average Decorrelation Level	29
12. PS Time Series From 1995 to 1997 Over Track 442	34
13. PS Time Series From 1997 to 2000 Over Track 442	35
14. PS Time Series From 1995 to 1997 Over Track 170	35
15. PS Time Series From 1997 to 2000 Over Track 170	36
16. GPS Displacements at the PBL	38
17. Spatial Average of Decorrelation Level	43
18. Cumulative Rainfall at the Portuguese Bend	45
19. Average Decorrelation Level with Average Rainfall	45
20. Landslide Velocity as a Response to Lag Time	47
21. Modeling Results Using a Four Week Lag Time	49
22. Modeling Results Using a Two to Six Week Lag Time	50

LIST OF TABLES

Table	Page
1. Summer Interferogram Dates	21
2. Landslide Parameters at the PBL	48

CHAPTER I

INTRODUCTION AND BACKGROUND

Project Motivation

Landslides occur frequently in mountainous, fluvial, and coastal settings, often incurring substantial damage or loss of life. Detecting and monitoring slides, however, can be both difficult and costly. Recent advances in interferometric synthetic aperture radar (InSAR) have shown much potential in identifying and quantifying landslides (*Hilley et al.*, 2004). The Portuguese Bend landslide (PBL) is a slow moving landslide that has much popular appeal, and numerous geological and engineering studies have been conducted over the past several decades (*Merriam*, 1960; *Bryant*, 1982; *Vonder Linden*, 1989; *Ehlig*, 1992; *Kayen* 2002). Despite an abundance of available satellite scenes, there has been no InSAR study of the PBL to date, perhaps due to the difficulty in observing the large magnitude surface deformation which is characteristic of the slide. In this study, I work around some of the difficulties in quantifying the high displacement rate, and ultimately apply the results to the mechanics of the landslide. The following sections describe the setting, geology, history, and mechanics at play at the PBL.

Study Area and Geologic Setting

The Portuguese Bend landslide is located on the southwest coast of the Palos Verdes Peninsula, 34 kilometers south of downtown Los Angeles (Figure 1). The bedrock underlying the Palos Verdes Peninsula is composed primarily of Mesozoic Catalina Schist, which is exposed on the northeastern face. The marine Monterey Formation overlays the schist, and is predominantly composed of Altamira Shale (*Vonder Linden*, 1989). This shale is the primary rock type associated with the landslides. In addition, there are volcanic rocks and coastal deposits which were created concurrently with the shale. At the base of the landslide is a layer referred to as the Portuguese Tuff which has largely altered to bentonite due to chemical weathering (*Ehlig*, 1992).



Figure 1. Study area: the Palos Verdes Peninsula. The Palos Verdes peninsula lies southwest of the LA basin in southern California. The inner red box identifies the region containing the landslide complex.

The Palos Verdes peninsula began uplifting in the Pliocene while below sea level as part of the Channel Islands. It remained an island until the late Pleistocene, at which

point it connected to the mainland just southwest of what is now Los Angeles (*Vonder Linden*, 1989). The anticlinal ridge which makes up most of the peninsula has marine terraces carved along the flanks which continue to be eroded today.



Figure 2. Study area: the Portuguese Bend landslide. A map of the entire landslide complex on the southwest coast of the Palos Verdes peninsula. The Portuguese Bend landslide is highlighted in yellow, the Abalone Cove in green, the Klondike Canyon in cyan, the Flying Triangle in blue, and the remainder of the Pleistocene landslide complex in red. Image courtesy of Google Earth.

The PBL covers an area of 1.06 km^2 , and it is part of a larger complex of landslides with an area of 6 km^2 . In addition to the PBL, this complex includes the Abalone Cove landslide to the west, the Flying Triangle landslide to the northeast, and a large area of ancient landslides to the north (*Ehlig*, 1992). The Portuguese Bend landslide lies just east of the distinctive Portuguese and Inspiration Points (Figure 2).

History of Landslides and Mitigation Attempts

The earliest sliding on the Palos Verdes Peninsula began upslope of the current active slide about 600,000 years ago (*Bryant, 1982*). The majority of slides on this ancient complex, however, did not initiate until about 120,000 years ago, when high sea level eroded the area around Portuguese and Inspiration Points (*Ehlig, 1987*). According to carbon-14 dating, the most recent ancient slides occurred around 4,800 years ago, and were likely caused by the erosion of the toe of the Pleistocene slide (*Emery, 1967*).

In 1956 the Portuguese Bend Landslide was reactivated. Despite knowledge of the ancient slide (*Kew, 1926; Woodring et al., 1947*), construction crews extending a road from the town of Rancho Palos Verdes dumped large amounts of fill to flatten the roadbed. In some areas they placed as much as 20 meters of fill, adding a significant load to the slope. Simultaneously, extensive new housing developments in the area raised the water table through landscaping practices and newly installed septic systems (*Ehlig, 1992*). Within months of the fill placement, the slide moved at a rate of several centimeters per day (*Vonder Linden, 1989*). The movement over the next several months destroyed 130 homes, 81% of the total residential block. Litigation following the initiation of the slide led to a study into the cause of recent motion. Taking into account the consultation of several geologists and engineers, the court eventually held the city liable for the damages caused to the houses, stating that the road construction had initiated the slide (*Vonder Linden, 1989*). The city was fined upwards of \$15,000,000, and in response, new building guidelines and restrictions were put in place. The incidents

surrounding the PBL brought engineering geology both into the public eye and into public works (*Ehlig*, 1992).

Since the initiation of the slide, deformation of the PBL has continued at rates varying with the seasons and rainfall levels. Other slides in the ancient landslide complex have also been reactivated since 1956. In 1978 the Abalone Cove Landslide just north of Portuguese Point began to move, and in 1980 a small portion of the Flying Triangle Landslide re-initiated as well. The Flying Triangle Landslide enlarged greatly in 1983, and continued to slide into the early 1990's (*Ehlig*, 1992). The Abalone Cove Landslide was stabilized in the early 1980's through dewatering techniques. Similar techniques were attempted on the PBL, but were less successful (*Ehlig*, 1992). The permeability of the PBL is lower than that of the Abalone Cove slide, so wells were not able to pump out significant amounts of water. In addition, the high deformation rate at the PBL quickly clogged and destroyed well casings (*Hill*, 2000).

Following extremely heavy rains and the subsequent acceleration in displacement in the late 1970's and early 1980's to rates of several meters per year, city engineers regraded much of the PBL and installed a second set of wells, along with storm drains to divert runoff directly to the ocean. Despite the fact that some water still entered the slide through surface fissures, the highest sliding rates were successfully reduced (*Kayen*, 2002). In 1988 engineers installed wire-mesh gabions at the toe of the PBL to slow wave erosion, but many of these were destroyed by storms the following year.

The mid-1990's brought some of the highest rainfall levels recorded in the 121-year history of Los Angeles, including the El Niño event over the winter of 1997-1998.

As in the late 1970's, this increase in rainfall corresponded to an acceleration in displacement, although the dewatering techniques were able to curb the most intense motion, keeping the maximum displacement levels below those reached previously. Following the El Niño event, displacement decelerated rapidly into the new millennium (Kayen, 2002). Between 1956 and 2002, Kayen (2002) reports that the landslide traveled an average total horizontal distance of 150-175 meters for an average displacement rate of 3.3 to 3.8 m/yr.

Properties of the Portuguese Bend Landslide

The Portuguese Bend Landslide is characterized as a deep seated landslide (Vonder Linden, 1989). The failure surface of the slide has a bedding plane angle which varies from 22° at the highest point to about 6° on the main portions of the slide (Ehlig, 1992). The eastern section of the slide is underlain with Miocene sedimentary bedrock, while the western section is underlain by moderately stable ancient landslide deposits. The thickness of the slide varies from several meters to 75 meters, and averages about 18 meters (Vonder Linden, 1989). The primary method of displacement in the PBL is block glide, and the failure surface is distinct and continuous (Ehlig, 1992; Vonder Linden, 1989). As the modest success of the dewatering campaigns and rainfall driven acceleration suggest, the landslide depends greatly on groundwater and pore pressure (Ehlig, 1992). Before dewatering attempts, Vonder Linden (1989) observed a velocity increase within 24 to 48 hours after a major storm. Multiple studies (Merriam, 1960;

Vonder Linden, 1989; *Ehlig*, 1992) agree that the displacement continues due to the constant coastal erosion at the toe of the slide.

The Portuguese Bend is a hydrologically driven, slow-moving, block-glide type landslide (*Ehlig*, 1992). Rainwater percolates down through cracks, fissures and pore space in the slide, raising the water table and increasing pore pressure throughout the depth of the slide. The bottom of the slide is bound by the Portuguese Tuff aquiclude which prevents further downward flow (*Ehlig*, 1992). The basic response of the slide can be understood using a landslide model first proposed by *Terzaghi* (1950), and recently quantified by *Iverson* (2000). The pore pressure increase reduces the normal force at the base of the block, lowering friction and causing the slide to accelerate downslope as a single unit. *Iverson* (2000) assessed his model in relation to the Minor Creek landslide in northern California and an experimental landslide facility. His theoretical model predicts a relationship between the landslide velocity as a function of the rainfall. This model incorporates physical parameters such as hill slope and slide depth, and soil properties such as angle of friction, soil weight, and diffusivity.

Thesis Overview

In this study, I use Interferometric Synthetic Aperture Radar (InSAR) and Global Positioning Systems (GPS) data to analyze the Portuguese Bend landslide and the area surrounding it. Multiple processing methods including conventional InSAR and permanent scatterers image the deformation, and constrain variables such as summer displacement rate and the time of rapid surface acceleration and deceleration in the fall

and spring. Using a landslide dynamics model proposed by *Iverson* (2000), I use my InSAR observations to estimate the hydraulic diffusivity of the slide mass, which governs slide response to rainfall events.

CHAPTER II

REVIEW OF PREVIOUS WORK ON THE PBL AND INSAR TECHNIQUES

Overview

The Portuguese Bend landslide is a well studied feature that has been monitored extensively due to its hazard potential to the community. Currently, researchers undertake regular GPS campaigns on and around the slide. InSAR is a burgeoning technique ideal for measuring how the surface of the earth changes over time. To date, however, no InSAR study has been published on the PBL. The following sections review important background information and previous work on the Portuguese Bend itself, and how InSAR has been applied to other landslides.

Previous Work on the Portuguese Bend

Initial studies by *Kew* (1926) and *Woodring et al.* (1946) identified the Portuguese Bend as the site of an ancient landslide complex, however, the potential for slope failure was not appreciated by landowners or city planners at the time. The reactivation of the slide in the 1950's initiated a reanalysis of the slide by *Merriam* (1960). In his report, Merriam defined the boundaries of the slide, proposed likely causes of reactivation, and observed displacement on and around the PBL. The report raised all of the vital issues

concerning the geologic controls on the slide mechanics. Several years later, *Vonder Linden* (1972) expanded previous studies by incorporating a plethora of borehole and well data. Collaborating with Lindvall, the report was republished in 1989 with an addendum including updates on the previous 15 years of slide activity. Perry Ehlig performed perhaps the most extensive work on the slide complex, with numerous papers on the mechanics of the Portuguese Bend and Abalone Cove landslides (*Ehlig*, 1982; *Ehlig*, 1986; *Ehlig*, 1992). Most of his work was completed in the late 1980's, culminating with the publication of his seminal piece, *Evolution, Mechanics and Mitigation of the Portuguese Bend Landslide, Palos Verdes Peninsula, CA*, in 1992. In this study, Ehlig summarizes all the previous work the PBL, the geology of the region, sliding history, current sliding rates and mechanisms, and mitigation attempts. Since 1992 no major studies have been published on the PBL in the scientific literature. *Kayen* (2002) present more recent data on displacement rates at the PBL, but their study primarily focuses on offshore sediment deposition on the Palos Verdes margin. Some recent work has been done by private consultants working for the city of Rancho Palos Verdes to monitor recent mitigation attempts and update the status of the development moratorium.

The PBL has been monitored since 1994 using a network of several dozen GPS benchmarks, which I have incorporated into this study. The data was collected by a private firm and has been provided by Dr. Robert Douglas at the University of Southern California. The data were collected at various times from 1994 to 2005, with periods

ranging from one day to a full year. GPS data supplement and validate results found through analysis of InSAR data.

Satellite Interferometry

My primary observation method for this study is Interferometric Synthetic Aperture Radar (InSAR). InSAR processing has many benefits for measure surface deformation. The displacement field obtained from conventional InSAR methods is continuous with a pixel resolution of ~30 meters. The sampling of the deformation field is much higher than would be acquired with a dense GPS network, for instance. Additionally, InSAR yields line-of-sight displacement values accurate to the sub-centimeter scale. Since the LOS vector is close to vertical with a look angle of $\sim 20^\circ$, InSAR is most sensitive to vertical deformation, which is the component least resolved by GPS (*Mao et al.*, 1999). Finally, InSAR data is collected monthly over each track, providing regular observations.

To create an interferogram a satellite reflects radio waves off of the Earth's surface at two separate times, recording the amplitude and phase of the returning signal each time. The reflected chirps are then projected back to the individual scatters on the ground, using the doppler shift and two-way travel time, and then the phase is interfered (*Bürgmann et al.*, 2000; *Hanssen*, 2001). The resulting phase shift indicates the distance the target has moved toward or away from the satellite as well as the surface height of the target from a reference ellipsoid. By removing the topographic signal in the phase using a DEM, the surface deformation is revealed. Due to the close proximity of the Portuguese

Bend to Los Angeles and its fortuitous placement with respect to the ERS satellites' trajectory, there are over 100 readily available scenes of the region on two satellite orbit tracks, 170 and 442. Since the two tracks overlap the region, data is available as frequently as every two weeks.

Several InSAR studies have been performed for the Las Angeles Basin, which includes the Palos Verdes peninsula (*Bawden et al.*, 2001; *Watson et al.*, 2002; *Lanari et al.*, 2004; *Li et al.*, 2005; *Brooks et al.*, 2007). Despite this, no InSAR study has focused on the PBL prior to this thesis. Using InSAR and MODIS data, *Li et al.* (2005) looked at the characteristic atmospheric signal over the entire Palos Verdes peninsula. They did not, however, examine the surface displacement of the slide itself.

The lack of recent studies may be due in part to the difficulty in using InSAR to image the large deformation rates of the landslide. The change in phase observed by the satellite cycles from 0 to 2π , and conventional InSAR requires that the change in phase from one pixel to the next is less than 2π radians, otherwise an ambiguity in the number of phase cycles exists (*Hanssen*, 2001). One phase cycle of 2π corresponds to 2.8 cm of deformation along the satellite line-of-sight. In cases of very high strain, the observed phase change may cross this limit, becoming decorrelated over the deforming area.

Rather than disregard those interferograms with decorrelated patches over the slide, I use them to constrain the spatial and temporal boundaries of the PBL. *Zebker et al.* (1996) utilize a similar technique to map decorrelation caused by terrain modification on lava flows in Hawaii. The other weakness of InSAR data is the one-dimensional nature of the observed displacement field. Since the satellite always detects the study area with the

same viewing geometry, the three-dimensional displacement is projected on to the line-of-sight (LOS) vector from the satellite to the ground. There are established approaches to work around this restriction, such as using scenes from both ascending and descending tracks. However, ascending data is not available for the study area. Here, GPS data and topography are used to determine the orientation of the slide movement and convert the LOS observation to downslope movement.

Recently, several research groups have introduced a new processing approach that accommodates large displacement gradients and unconformities using permanent surface scatterers (*Ferretti, 2001; Colesanti et al., 2003; Hilley et al., 2004; Salvi et al., 2004; Hooper et al., 2006*). Unlike conventional InSAR processing, which unwraps continuously from pixel to pixel over the entire area, PS InSAR identifies strong surface reflectors and tracks their phase in time from one scene to the next. While conventional InSAR interferograms are unwrapped spatially, PS InSAR unwraps pixels in time. In the case of a landslide, this means that individual scatterers may unwrap coherently even if their phase is unrelated to nearby pixels with substantially different displacement rates.

Using InSAR to Monitor Landslides

InSAR is most commonly used to measure deformation fields caused by seismic events and aquifer subsidence (*Price, 1998; Bürgmann et al., 2000; Furuya et al., 2007, Finnegan et al., 2008*). Relatively little work has been done using InSAR to monitor landslides, as the large magnitude deformation rates associated with slides often makes conventional interferometry difficult or impossible. Most of the InSAR work on

landslides has been done by European research groups, primarily looking at mountainous slides (*Carnec*, 1996; *Fruneau*, 1996; *Ferretti*, 2001; *Squarzoni*, 2002; *Colesanti*, 2003; *Farina*, 2004; *Catani*, 2005). Conventional InSAR studies have primarily used short repeat-cycle data, collected either during the ERS commissioning phase in 1991 (3-day repeat cycles), or on TANDEM missions in 1995, 1996, 1997 and 1999 (1-day repeat cycles) (*Carnec*, 1996; *Fruneau*, 1996; *Squarzoni*, 2002). *Kimura et al.* (2000) examined a landslide in northern Japan using a multiple pass method with JERS L-band (23.5 cm wavelength) data. The permanent scatterers method has been the most popular approach for dealing with the large displacements typical of landslides. *Colestanti* (2003), *Hilley et al.* (2004), *Ferretti* (2005), and *Farina* (2006) have used permanent scatterers to successfully measure landslide displacement rates. Additionally, *Hilley et al.* (2004) relate sliding velocity in the Berkeley Hills of northern California to the lag time after the onset of the rainy season. Here I perform a similar analysis to estimate the hydraulic diffusivity at the PBL.

While some work has been done using InSAR to look at landslides, many aspects, such as mapping decorrelation, have gone largely unexplored. The popularity and extensive documentation of the Portuguese Bend make it an ideal site to test new techniques and methods.

CHAPTER III

ANALYSIS OF INSAR DATA FOR THE PALOS VERDES PENINSULA

Overview

I conducted this study of the Portuguese Bend Landslide using data from European Space Agency (ESA) satellite system ERS 1/2 collected between 1992 and 2001. The Palos Verdes peninsula lies within the region overlapped by two paths of the satellite (tracks 170 and 442), effectively making available twice as many scenes over the region as is typical for InSAR studies. For each track, the area of interest is contained entirely within frame 2925 (Figure 3). For track 170, 19 scenes collected by ERS-1 and 57 by ERS-2 are used. Over track 442, 21 scenes collected by ERS-1 and 36 by ERS-2 are used (Appendix A). In this chapter, I discuss the methods, analysis, and results of the study.

Interferogram Formation

SAR data are first processed using conventional interferometric techniques (Massonet *et al.*, 1993; Zebker *et al.*, 1997; Bürgmann *et al.*, 2000). The ROI PAC software suite is used to create single-look-complex (SLC) images from the raw ERS data (Rosen *et al.*, 2004). A 1 arc-second (30 meter resolution) digital elevation model

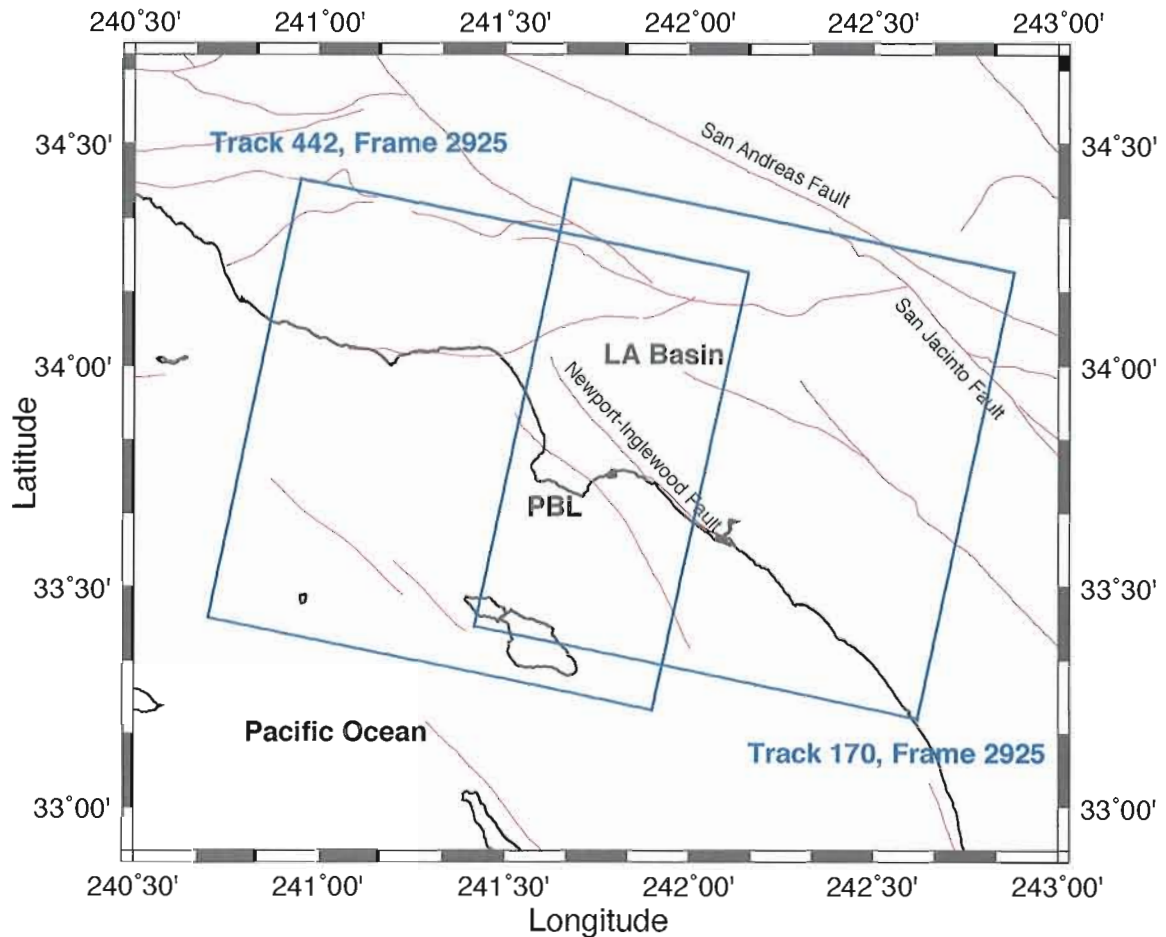


Figure 3. ERS satellite tracks. Track 170 frame 2925 and track 442 frame 2925 are outlined in blue over the Los Angeles basin. The PBL is on the southwest edge of the Palos Verdes peninsula. Major faults are marked in red (*Jennings, 1994*).

(DEM) created by JPL from data collected during the Shuttle Radar Topography Mission (STRM) is used to remove the topographic component of the phase. All scenes are processed at 4-looks resolution, and otherwise used standard values for the processing parameters. Only pairs of scenes with perpendicular baseline values of less than 200 meters are processed in order to avoid coregistration difficulties in ROI PAC. In the end, 288 interferograms were processed on track 170, and 251 were processed on track 442.

Track 442 primarily covers the coastline west of the LA basin, with the Palos Verdes peninsula in the right-center of the frame. Track 170 is centered over the LA basin, with the peninsula on the far left side of the frame. Interferograms from both tracks show generally poor coherence in the mountains and hills, high coherence in the urban areas, substantial atmospheric artifacts, subsidence in previously studied basins (*Bawden et al.*, 2001), and deformation along the Newport-Inglewood fault which runs just north of the peninsula (*Watson et al.*, 2002).

Over the Palos Verdes peninsula, the database of interferograms exhibit three characteristics which complicate the data set, and have forced unconventional examination of the data. First, many interferograms display a strong phase signal along the northwest to southeast trending ridge of the peninsula, which is uncorrelated to any expected surface deformation. This signal is likely explained as an atmospheric artifact. Second, the interferograms do not exhibit a clear signal around the landslide area. Finally, most interferograms lose phase coherence near the slide, though the extent of the decorrelation varies.

Atmospheric Artifacts

Many interferograms show a broad phase signal extending northwest to southeast along the length of the Palos Verdes peninsula. The same signal is described and analyzed by *Li et al. (2005)*, who attributed it to variations in the concentration of water vapor in the atmosphere. Using InSAR, MODIS and GPS data, they use water vapor content data to predict the signal delay caused by the atmosphere, and remove it from the

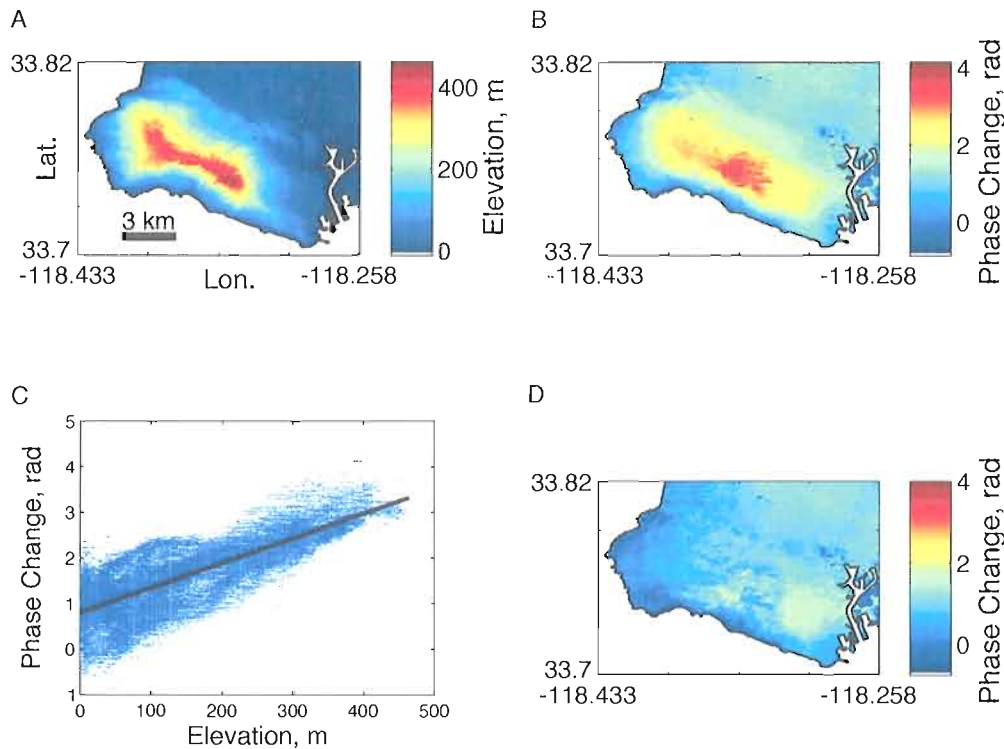


Figure 4. Removing atmospheric artifacts. (A) Digital elevation model of the Palos Verdes peninsula, southern California. Elevation reaches a maximum of 460 meters atop the northwest to southeast trending ridge. (B) 11/11/1999 - 12/16/1999 interferogram before the topographically correlated atmospheric signal is removed. (C) The phase at each pixel for the 11/11/1999 - 12/16/1999 interferogram plotted against the corresponding elevation from the DEM. To first order, this signal correlates very well to the elevation of the ridge, with higher elevations exhibiting a greater phase change. The best linear fit is plotted in black. (D) 11/11/1999 - 12/16/1999 interferogram after the topographically correlated atmospheric signal is removed.

interferogram phase. The broad atmospheric phase artifact corresponds well to the topography along the length of the peninsula, as the northwest to southeast trending Palos Verdes Hills rise from sea level to 450 meters at their peak (Figure 4.A).

I interpret the broad phase signal as a result of vapor-rich air blowing off the ocean in the form of fog that hugs the ridge line. The high moisture content slows the electromagnetic wave in the column of air surrounding the ridge, resulting in a broad,

distinct signal (*Hanssen et al.*, 1999). To remove the signal, each interferogram is examined individually by plotting the phase of each pixel against the corresponding elevation from the DEM (Figure 4.C). After solving for the best linear fit through the scatter of points, the atmospheric component is estimated and removed from the phase. The result is a much cleaner interferogram with no topographically correlated signal (Figure 4.B, 4.D). Any signal representing deformation of the surface (such as due to landsliding) should be unaffected by this correction.

Stacking Interferometric Pairs

Even with the broad atmospheric signal removed, individual interferograms often do not show a signal over the landslide area that is significantly larger than the magnitude of artifacts. Most of the interferograms are partially incoherent over the sliding area, and interferograms that are completely coherent typically span a short time period (35-105 days), typically in the summer months. The lack of obvious deformation in the coherent interferograms is due to the fact that the signal to noise ratio is low. The short temporal baseline and low sliding velocity in the summer months reduce the deformation observed in any single interferogram to near or below the magnitude of artifacts, such as from atmospheric effects (Figure 5).

In order to better visualize the deformation in the study area and reduce the effects of artifacts, I employ a stacking algorithm to accentuate deformation with amplitude similar to noise. In stacking the data, the mean phase value is first removed from each

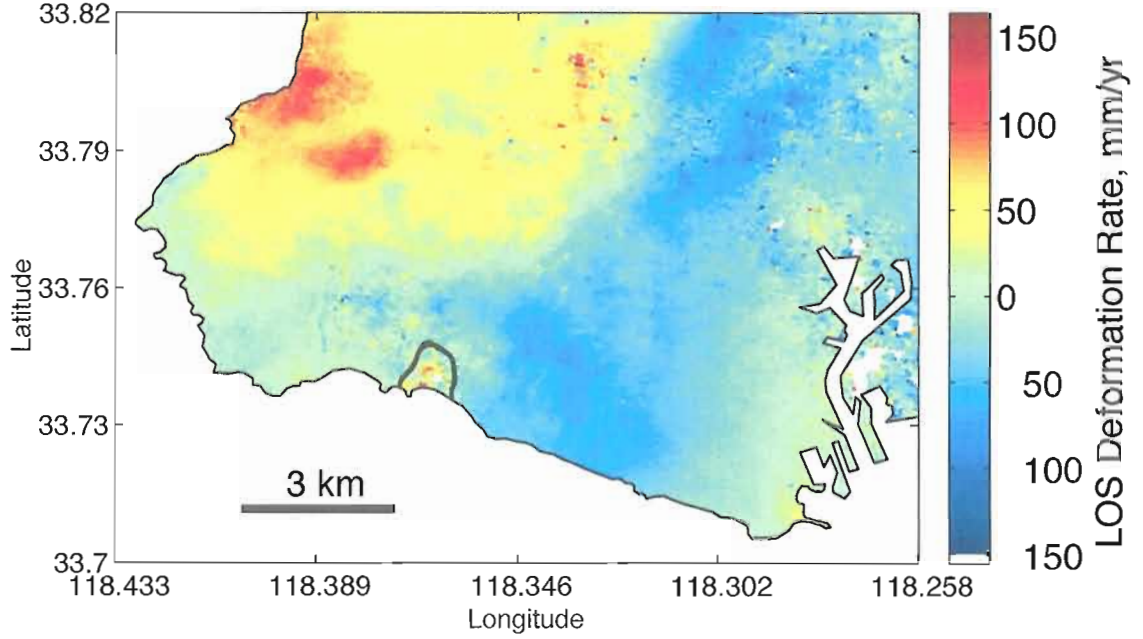


Figure 5. 08/09/1997 - 09/13/1997 interferogram exhibiting deformation at the PBL which is about the same magnitude as noise. This is typical of summer interferograms. The maximum extent of the Portuguese Bend landslide is outlined in black.

interferogram. Then for each pixel, the phase change for all interferometric pairs is summed and divided by the entire length of time elapsed. For the i^{th} pixel:

$$\Phi_i = \frac{\sum_{n=1}^n \varphi_{n,i}}{\sum_{n=1}^n \Delta t_{n,i}} \quad (1)$$

where Φ_i is the total phase change, $\varphi_{n,i}$ is the phase of the n^{th} interferogram, and $\Delta t_{n,i}$ is the time span of the interferogram. If a pixel is incoherent for a certain interferogram, the algorithm removes that value from both the phase and time terms.

Using 33 synthetic aperture radar (SAR) scenes, 20 independent interferograms are created (Table 1). These interferograms are combined into two stacks, one for track

Track 170		Track 442	
Starting Date	Ending Date	Starting Date	Ending Date
Apr 21, 1995	May 26, 1995	Apr 5, 1995	Jun 14, 1995
Jun 30, 1995	Sep 8, 1995	Jun 14, 1995	Jul 19, 1995
Apr 6, 1996	Sep 28, 1996	Jun 14, 1995	Aug 23, 1995
Apr 26, 1997	May 31, 1997	Aug 23, 1995	Sep 27, 1995
May 31, 1997	Jul 5, 1997	Jul 4, 1996	Oct 17, 1996
Aug 9, 1997	Sep 13, 1997	May 15, 1997	Jun 19, 1997
Sep 13, 1997	Oct 18, 1997	Jun 19, 1997	Jul 24, 1997
Apr 11, 1998	Jul 25, 1998	May 4, 2000	Jun 8, 2000
May 16, 1998	Jun 20, 1998		
Jun 20, 1998	Oct 3, 1998		
May 1, 1999	Oct 23, 1999		
May 20, 2000	Sep 2, 2000		

Table 1. Summer interferogram dates. For frame 2925, the starting and ending dates for the 20 interferograms used in the summer stacks over tracks 170 and 442.

170 and one for track 442. The data from each track must be stacked separately because of the difference in look angle.

Interferograms are selected such that the starting and ending dates are confined to a single year between the months of April and October. These are the months which most consistently remain coherent over the sliding area. The result of the stacking is clearly defined deformation at the Portuguese Bend. The deformation rates over the landslide are 45.8 ± 13.9 mm/yr for track 170 (Figure 6) and 54.7 ± 16.4 mm/yr for track 442 (Figure 7) along the satellite line-of-sight. The high standard deviation is due to annual variations in the sliding rate, with some years exhibiting more deformation than others. The process

of stacking the data has also greatly reduced the background artifacts in non-deforming regions.

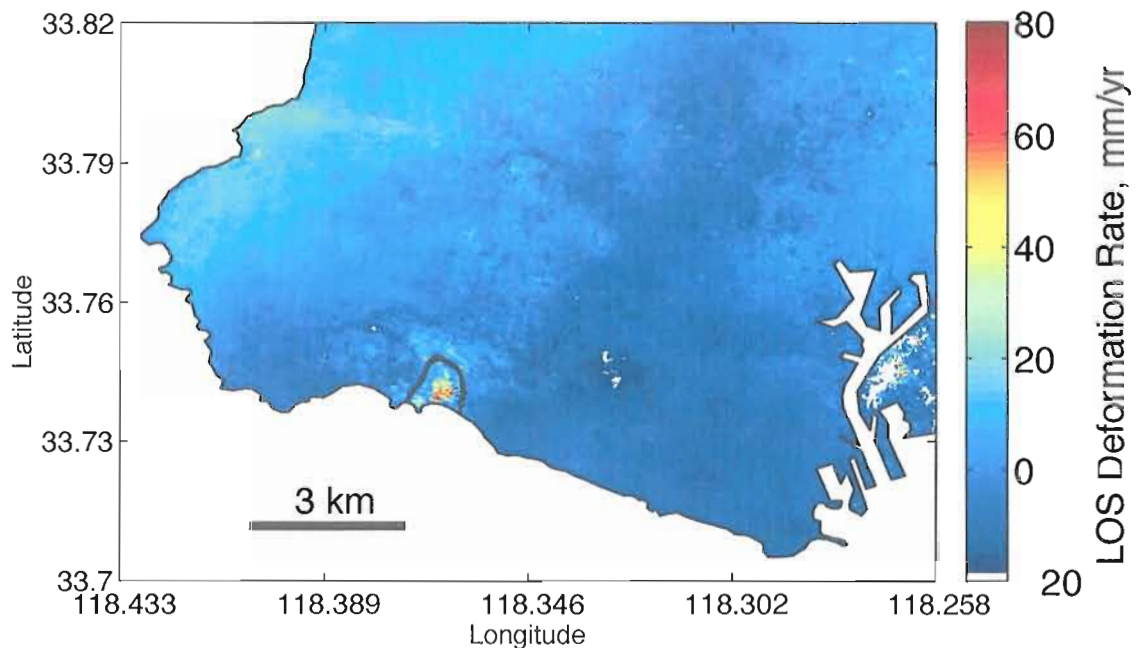


Figure 6. Stack of 12 summer interferograms for track 170 between 1995 and 2000, listed in table 1. The previously mapped maximum extent of the PBL is outlined in black.

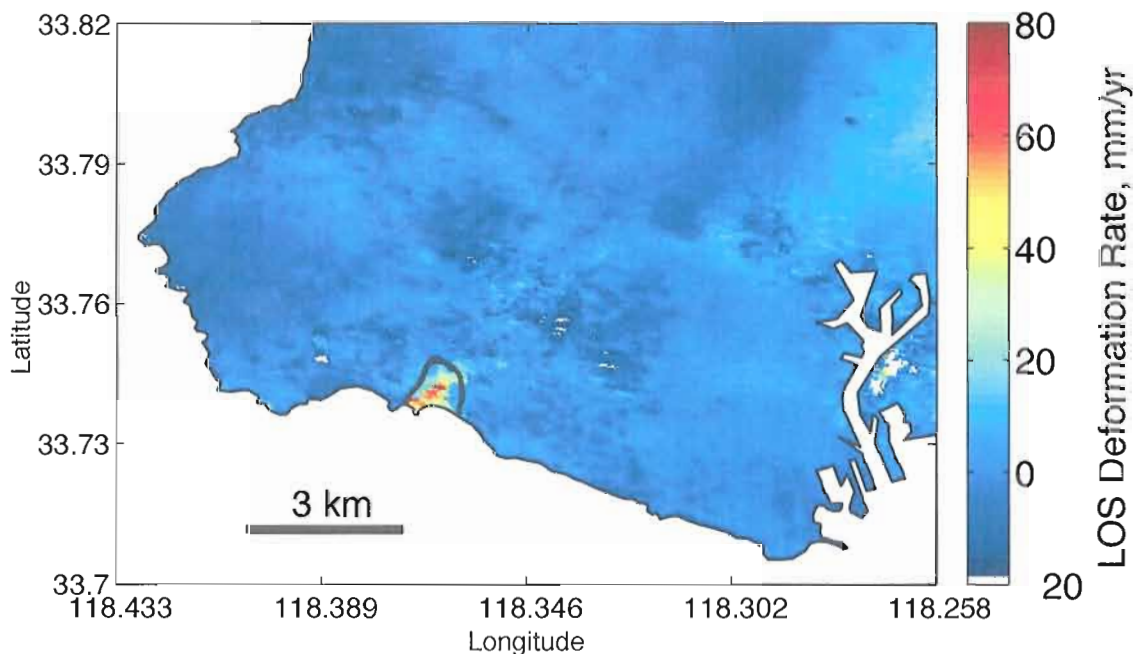


Figure 7. Stack of 8 summer interferograms for track 442 between 1995 and 2000, listed in table 1. The previously mapped maximum extent of the PBL is outlined in black.

Quantifying Interferogram Decorrelation

Many interferograms of the Palos Verdes peninsula spanning more than the summer months show pockets of decorrelation on and around the mapped area of the PBL. Decorrelated pixels identify areas where the phase is not spatially correlated to neighboring pixels. Decorrelation is caused by low coherence, γ , which can be quantified using the following expression:

$$\gamma = \frac{\langle c_1 c_2^* \rangle}{\sqrt{\langle c_1 c_1^* \rangle \langle c_2 c_2^* \rangle}} \quad (2)$$

where c_i is the complex phase for scene i , c^* is the complex conjugate, and $\langle \rangle$ represents spatial averaging. Generally pixels of low γ (<0.4) are ignored in studies because they do not showing quantifiable evidence for deformation (Baran, 2005). Here, enough interferograms with decorrelated patches are combined to derive useful information about the spatial and temporal extent of rapid ground movement associated with the PBL.

Phase decorrelation can be caused by several different phenomena. Anything that makes the raw phase signal speckled, or that pushes phase fringes too close together will create an incoherent patch. One common cause for incoherence is vegetation (Zebker *et al.*, 1992). From one scene to the next, vegetation may grow, shift in the wind, or change in shape. Each of these will alter the pattern of surface scatterers within a pixel footprint and reduce the phase coherence between scene acquisitions (Zebker *et al.*, 1992). Where not developed, the Palos Verdes Peninsula is sparsely vegetated with coastal sage scrub and non-native grass species (Munz, 1979; Gabet, 2002). The largest vegetated areas are on the southwest coast of the peninsula, including the PBL and surrounding areas. The

city has placed development restrictions on this land because of current and recent landsliding and evidence of ancient landslides. The lack of decorrelation in similarly vegetated areas around the PBL rules out vegetation as the main cause of decorrelation over the PBL for short time span interferograms (less than one year). The decorrelated patches are confined to the boundaries of the mapped landslide and do not extend into the surrounding areas. These surrounding areas maintain a coherent phase signal for time scales of less than one year, after which they become decorrelated as well. This longer time scale of decorrelation may be due to the cumulative effects of vegetation growth.

The major cause of decorrelation for short duration interferograms over the PBL is the steep deformation gradient along the edge of the landslide. The slide undergoes block-glide style deformation, with the entire area moving as a unit down slope with a small amount of internal deformation (*Ehlig, 1992; Vonder Linden, 1989*). Since the boundary zone where the slide ramps from zero deformation to the maximum sliding rate is small, the shear strain is quite large (~ 0.05 strain). Before unwrapping, the interferometric phase cycles from 0 to 2π , with a jump in the data every time a new cycle begins. This is the nature of SAR data, as the phase change measures the offset between primary and secondary electromagnetic chirps scattered from the surface at two separate times. Because the interferometric phase signal changes too quickly from the outside to the inside of the slide, the processing software is unable to successfully unwrap the phase as the algorithm approaches the interior of the slide, so the slide becomes decorrelated. The theoretical limit for unwrapping a steep phase gradient is 2π radians per pixel (*Massonnet et al., 1998*).

One other possible source of decorrelation at the PBL is internal deformation. If individual blocks of the slide move with respect to one another in a random fashion, the phase signal may be too complex to unwrap properly. Because the slide undergoes primarily block-glide motion, the steep deformation gradient along the edge of the slide is the primary challenge when unwrapping the data.

Temporal Mapping of Interferogram Decorrelation

The steep deformation gradient which causes decorrelation at the PBL is along the margins of the slide (Figure 8). In each interferogram, the decorrelated patch is used to identify where the deformation gradient is large enough to have crossed the phase gradient unwrapping threshold. Stacking decorrelated patches from many interferograms gives an approximate outline of the entire slide.

The greatest amount of decorrelation occurs during the winter months, and in many cases it expands beyond the borders of the mapped landslide. Interferograms with a temporal baseline greater than one year are completely decorrelated over the sliding area, with the decorrelation generally extending to the borders of the undeveloped region of the peninsula (Figure 9). This is interpreted as a result of vegetation growth, as described in an earlier section. To limit the bounds of the landslide, therefore all interferograms spanning more than twelve months are excluded from the forthcoming analysis.

The stacking method used here yields information on both the spatial and temporal characteristics of the PBL. A given pixel becomes decorrelated if $\gamma < 0.4$. For each day of the year, the decorrelation level, I , is the ratio of the number of

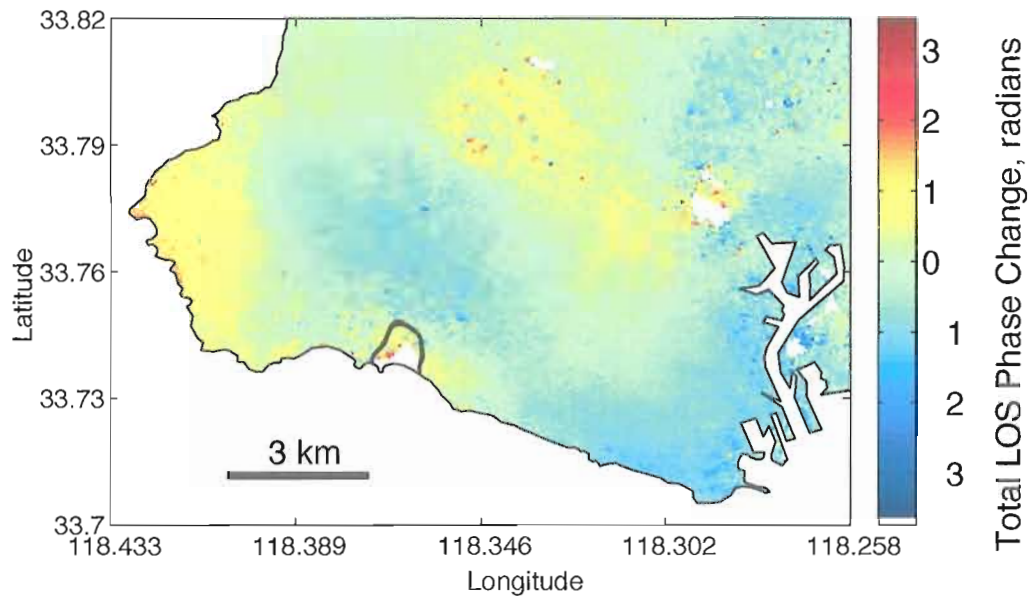


Figure 8. 12/23/1995 - 01/27/1996 interferogram shows decorrelated patches typical of winter interferograms. The area immediately over the landslide is decorrelated, while the surrounding area maintains phase coherence. The previously mapped maximum extent of the PBL is outlined in black.

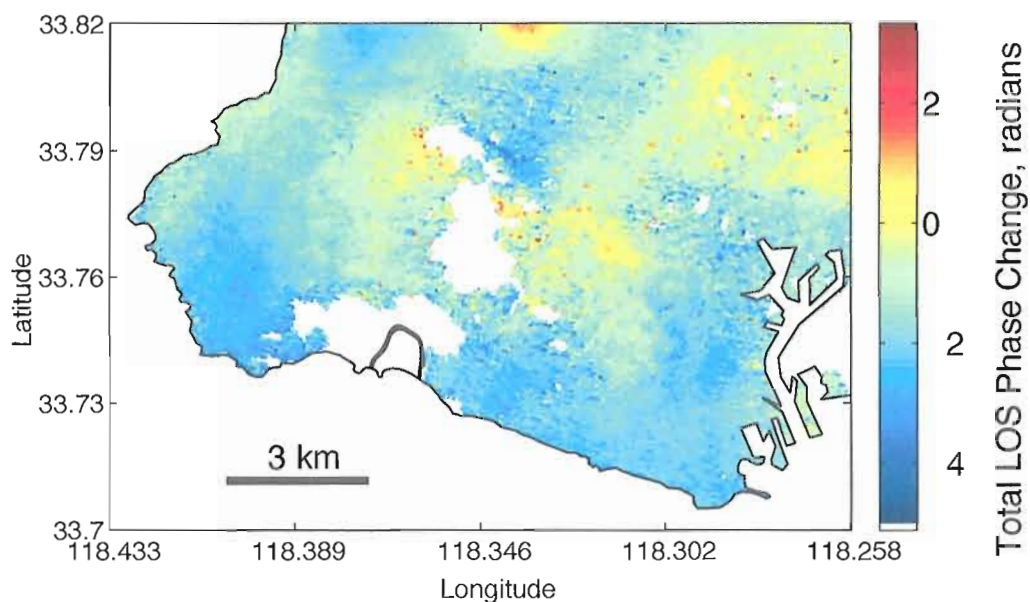


Figure 9. 05/16/1998 - 06/05/1999 interferogram shows large decorrelated patches over the vegetated regions of the peninsula. This is typical of interferograms longer than one year. The previously mapped maximum extent of the PBL is outlined in black.

interferograms in which a certain pixel is decorrelated to the number of total interferograms containing that day:

$$I_{t,i} = \frac{n_{t,i}}{N_{t,i}} \quad (3)$$

where i is the pixel index, t is the day of the year, n is the number of decorrelated interferograms, N is the total number of interferograms containing day t . This method collapses all 9 years of data onto a single calendar year, which effectively yields a multi-year average for the decorrelation over the landslide. With this technique, coherence is mapped as a function of space and time.

Because decorrelation is caused when the phase gradient becomes too steep around the edges of the slide, no information is available for the slide interior. Therefore, rather than consider the maximum level of the decorrelation, the relative shifts in its level are indicative of displacement near the coherence threshold. When the decorrelation level ramps up sharply, it is a sign that the phase unwrapping threshold has been crossed. When it drops, coherence has been recovered and the slide has slowed enough to allow successful unwrapping. Using the theoretical threshold for phase unwrapping, the phase gradient is determined when coherence is lost or recovered. Finally, by applying data on the width of the borders of the slide, the phase gradient is converted to a displacement rate. The displacement rate at which the decorrelation level increases significantly is 2.5 m/yr. This analysis and calculation is described in depth in the next chapter.

This technique for decorrelation mapping is applied to 157 interferograms with temporal baselines less than one year. I find that the percent of pairs which are

decorrelated increases as one approaches the center of the PBL. Additionally, the decorrelation level both on and around the PBL increases in the winter months and decreases in the summer (Figure 10).

A decorrelation level of 0.8 means that 80% of the interferograms are decorrelated on that day for that pixel. The actual values for I are high (generally >0.7) because by using all interferograms with a temporal baseline less than one year, there are many pairs

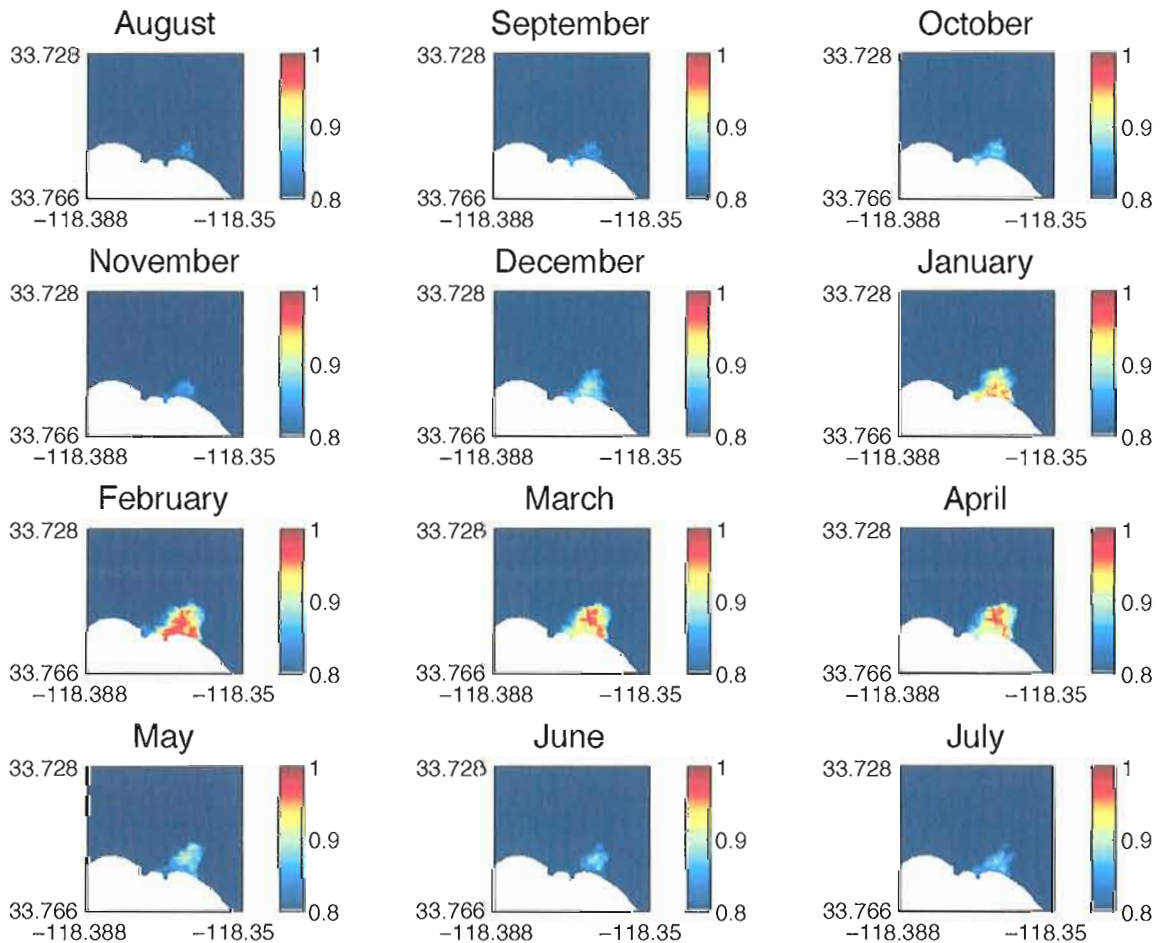


Figure 10. The decorrelation level mapped at the PBL. Blue areas have low levels of decorrelation, while red areas are decorrelated for nearly every interferogram in the date range. Several years of data are condensed onto a single calendar year. The decorrelation increases sharply in December and decreases in May.

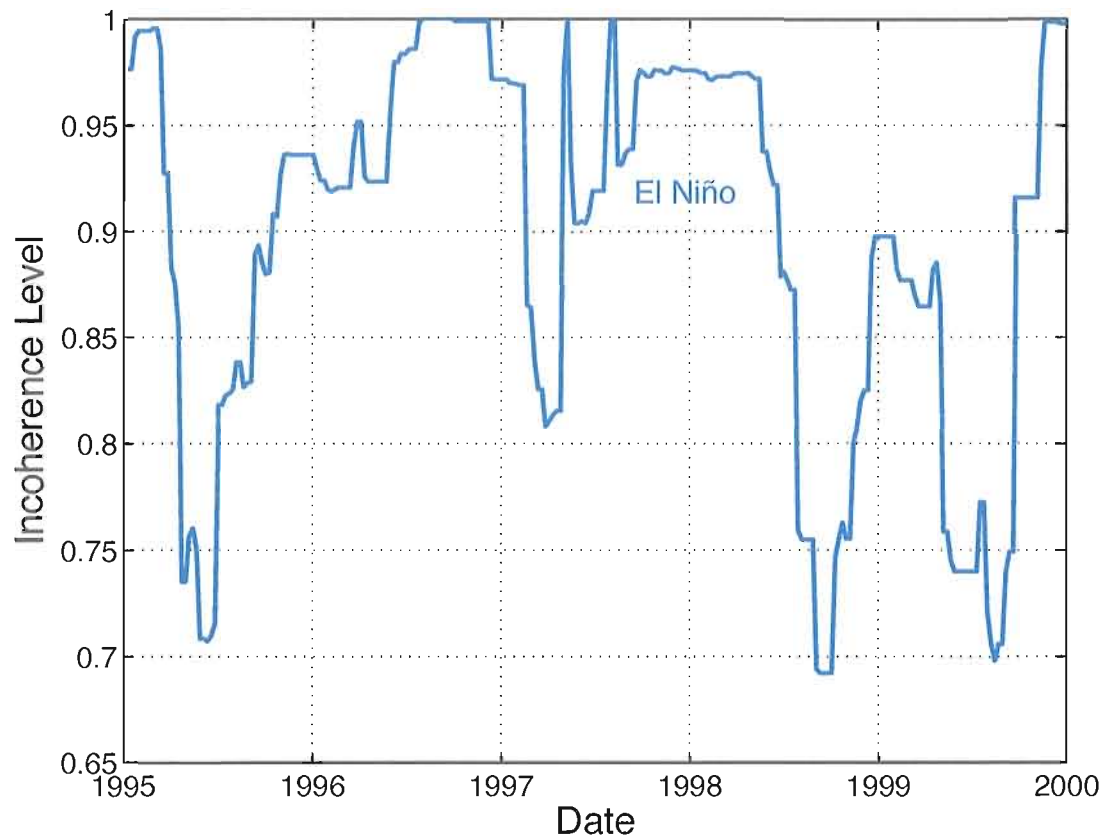


Figure 11. Full time series of average decorrelation level over the mapped landslide. The decorrelation level does not fall as expected during the summer of 1996 due to the lack of short time span summer interferograms and high rainfall. The El Niño year of 1997-1998 exhibits increased decorrelation level both in the fall and spring. The data is truncated at the start of 2000 because too few interferograms exist to resolve the decorrelation level.

containing both the winter and summer seasons. Although the decorrelation is caused by winter deformation, for these pairs it counts in the summer as well, increasing the final value for decorrelation level.

Stacking all of the data onto a one-year time frame is helpful for resolving the spatial evolution through the winter season. In order to visualize the annual changes from one year to the next, I plot the decorrelation level time series from 1995-2000 (Figure

11). Here, the plotted decorrelation level is a spatial average over all the pixels in the mapped landslide. This plot shows a substantial decrease in I during the summers of 1995, 1998 and 1999, but little decrease in 1996 and an earlier than expected drop in 1997. These two summers highlight the problems encountered by stacking the full time series. The temporal resolution for this method is reduced from the previous method which condenses all the data onto a single calendar year. Because new data arrives only twice every 35 days, once for track 170 and once for track 442, there are often too few scenes containing a specific date to obtain a meaningful decorrelation level, and I becomes highly dependent on individual scenes. For instance, if a date is bracketed by only three interferograms, the possible decorrelation levels are 0, 1/3, 2/3 and 1. Therefore, the results become more discretized and a small number of scenes bias the average. Despite these difficulties, some general observations can be made from this full time series. In general, decorrelation level drops significantly during the spring and increases sharply in late fall, however the decorrelation extends longer into the spring of 1998 than other years. This delay is attributed to the El Niño winter of 1997-1998 which prolonged the high sliding rate into the late spring.

Permanent Scatterers Method

The permanent scatterers method is a relatively new technique which has proved effective at monitoring landslides (Ferretti *et al.*, 2001; Hilley *et al.*, 2004). The sharp phase gradient around the edges of the PBL causes the unwrapping step in conventional InSAR processing to fail. The permanent scatterer method (PS InSAR) unwraps

individual points in time rather than space, which may allow for better resolution of the landslide deformation. Individual reflectors are selected from the single look complex (SLC) image based on two characteristics: they are stable in time, and they dominate the signal reflected back to the satellite within a footprint. There are several houses on the PBL which should act as strong reflectors, appearing in each scene and reflecting a relatively large amount of energy back to the satellite.

Conventional InSAR assumes that the phase is highly correlated among adjacent pixels. This condition is not met along the edges of the PBL where spatial gradients are high. PS InSAR has an advantage here by correlating pixels in time rather than in space. Even if the phase at interior points does not correspond well with that of points outside the boundary of the slide, they may nonetheless be identified as scatterers and be successfully unwrapped through the time series. This ideal result would yield a deformation rate for pixels on the slide through the entire year, including the fast deformation in the winter. Phase unwrapping restrictions still limit the maximum phase change at a certain pixel from one scene to the next. If the phase change is greater than π radians per epoch for unknown deformation direction (i.e., increasing or decreasing phase change), or 2π radians per epoch for known deformation direction, the phase cycle becomes ambiguous, and unwrapping becomes impossible (*Ferretti et al.*, 2003). To minimize this phase ambiguity in the presence of fast deformation, it is important to use SAR scenes with acquisition times as close together as possible.

The PS method used here, StaMPS, was developed by Andy Hooper and described in his 2006 dissertation and 2007 study of Volcán Alcedo. Unlike other PS

techniques, StaMPS does not assume a linear deformation rate, making it more appropriate for a seasonally dependent target like the PBL. Drawing from the same set of ERS scenes used for conventional processing, StaMPS is used to create four separate time series over the Palos Verdes peninsula, two for track 170 and two for track 442. For each track, the first time series is from 1995 to the end of 1997 and the second is from the end of 1997 to the beginning of 2000 (Appendix B). The master scenes are selected based on the criteria laid out in *Hooper et al.* (2007), minimizing the product of temporal baseline, perpendicular baseline, and the difference in doppler centroid between the master and each slave.

PS candidates are selected first by their amplitude dispersion, which is defined as the standard deviation of the series of amplitude values divided by the mean of the amplitude values. All points below a threshold of 0.4 move on to the next selection process where they are tested for phase stability. After an iterative process that gradually weeds out pixels which fail the phase analysis, final PS points are selected. Most of the PS points selected by StaMPS are on the developed portions of the peninsula where buildings act as strong and stable reflectors. The density of points decreases over the vegetated area in the south center of the peninsula, which includes the Portuguese Bend landslide complex (Figures 12-15).

The PS analysis achieves various levels of success in terms of scatterer selection and deformation detection. The two 1997-2000 time series contain the most scatterers, with 40,990 selected for track 170 and 34,905 selected for track 442. These series work well because the master scene processes successfully with many available slave scenes,

allowing for a high scene density through time. The 1995-1997 series contain fewer scatters, with 20,681 PS selected for track 442 and only 5,448 selected for track 170. Track 170 has fewer scatterers because the series incorporates fewer scenes, making it more difficult for scatterers to move through the selection process. Because pixels are correlated through time, a higher scene density increases the phase stability, which allows more pixels to be identified as permanent scatterers. The slave to master perpendicular baselines vary substantially during this time span, so many of the slaves had to be removed during in the processing.

Each of the 1997-2000 PS series show a small amount of deformation in the area outside the mapped boundaries of the PBL. The range change is away from the satellite, and corresponds to about 8 mm/yr along the satellite LOS, or ~ 6 cm/yr along the slide displacement vector. I interpret this as deformation occurring on the currently active mapped landslides and ancient landslide complex neighboring the PBL. The displacement rate is an order of magnitude lower than at the PBL, and is confined to the no-build landslide moratorium area.

In each series there are very few PS points on the actual PBL. Given the relatively high density of points in the surrounding areas (including similarly vegetated regions), the lack of PS points may be more complicated than the simple lack of strong reflectors. Most PS candidates are dropped after phase stability is assessed, including nearly all points on the PBL. Because the expected deformation rate is so high across the slide itself, StaMPS may interpret the large deformation signal as unstable phase, removing potentially good scatterers. The few points that do fall on the landslide itself do not show

significant deformation, suggesting a failure in the unwrapping step. Examining the time series of raw phase values for these points, no clearly defined deformation rate can be discerned. The phase appears to cycle through more than 2π radians per epoch, making unwrapping impossible.

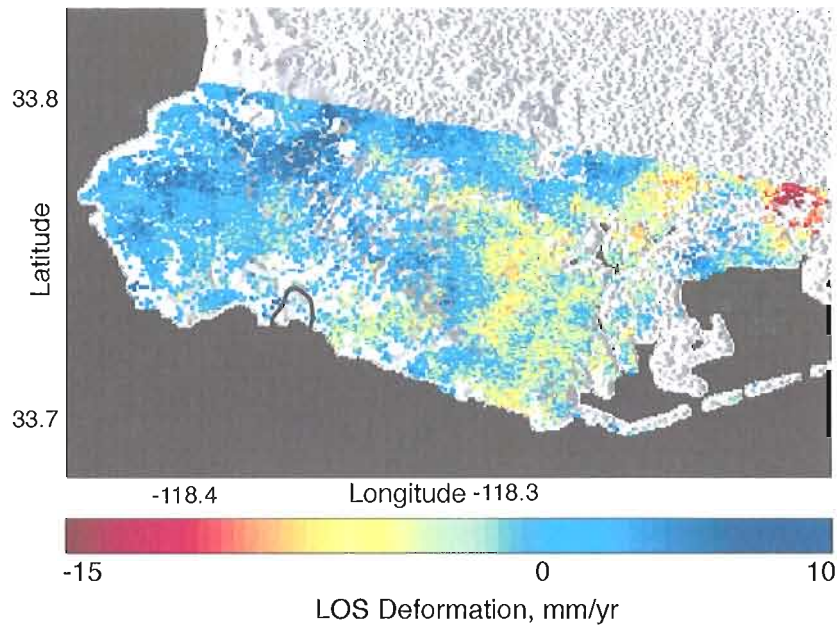


Figure 12. PS time series from 1995 to 1997 over track 442. The PS pixel density around the PBL is very low and pixels do not show significant deformation.

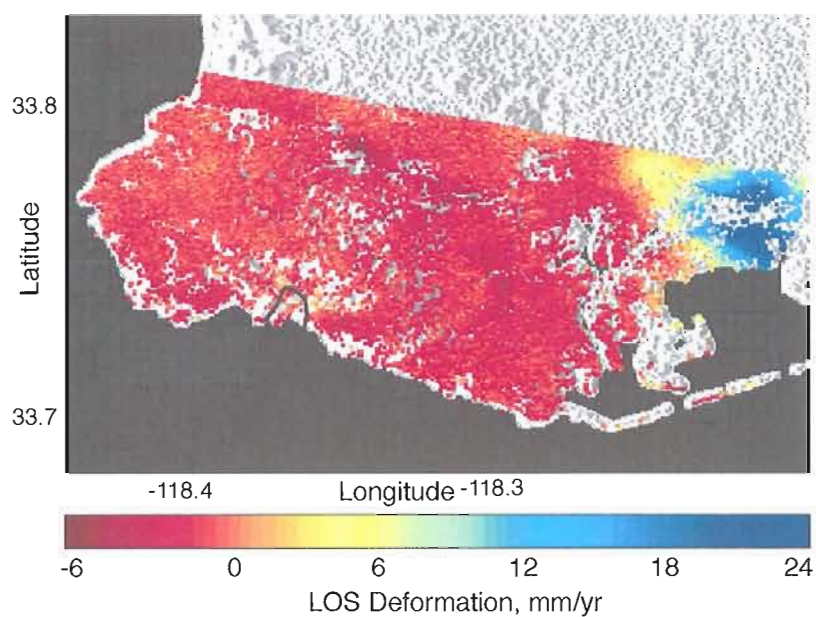


Figure 13. PS time series from 1997 to 2000 over track 442. Many scenes are used to create this series, increasing the density of PS pixels selected. Pixels surrounding the PBL show subtle deformation away from the satellite, but pixels on the slide itself show none.

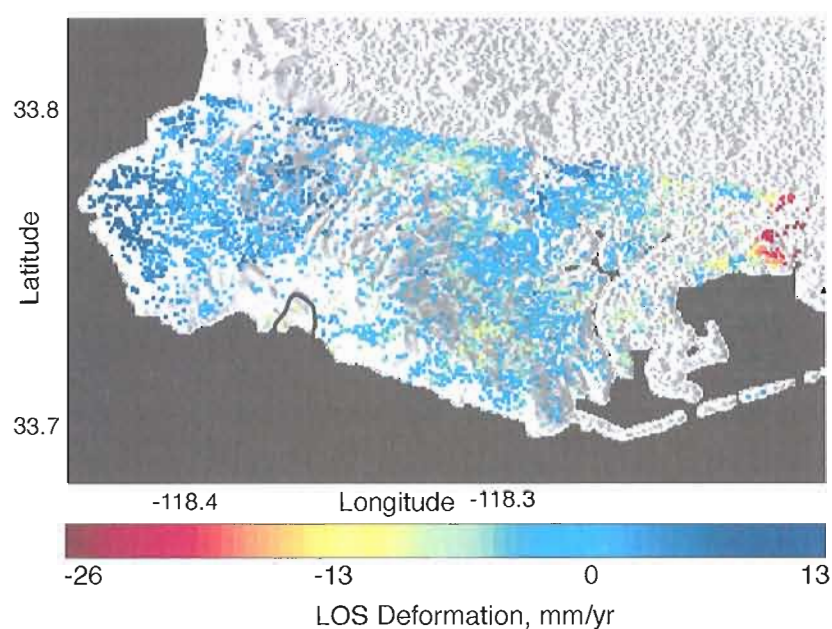


Figure 14. PS times series from 1995 to 1997 over track 170. Not enough scenes are available for this time period to achieve high PS density near the PBL.

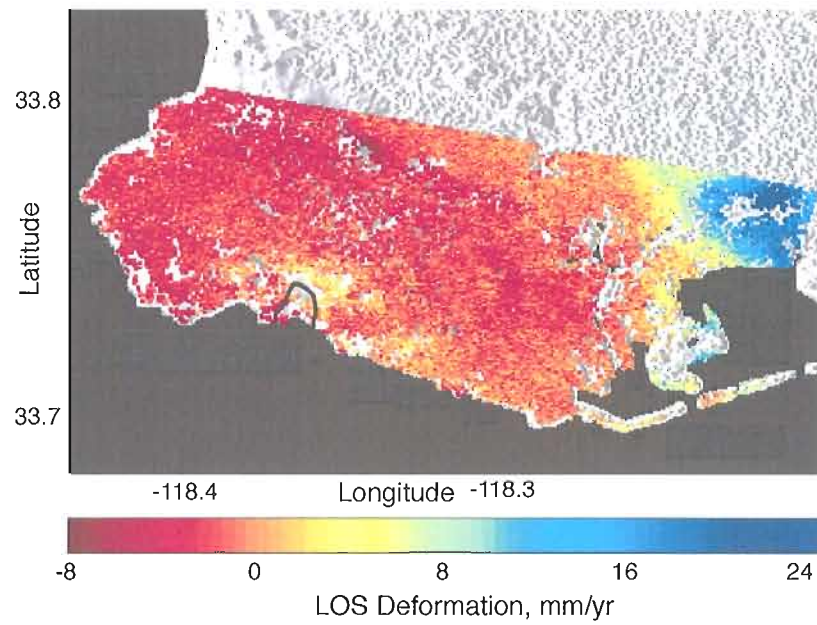


Figure 15. PS time series from 1997 to 2000 over track 170. The yellow pixels near the PBL show subtle deformation away from the satellite, which may be the result of low levels of deformation in the surrounding landslide complex. The PS pixels over the PBL itself do not show deformation, which is a result of an unwrapping failure.

CHAPTER IV

INTERPRETATION AND DISCUSSION OF INSAR RESULTS

Overview

In the previous chapter, I analyzed the ERS satellite data using various approaches in an effort to overcome difficulties in resolving a fast moving slide. These individual techniques also yield slightly different, though complementary, information about the Portuguese Bend landslide. By examining these results individually and in conjunction with one another, the slide's response to rainfall is assessed, and from that, physical parameters such as diffusivity are constrained. In this chapter, I take the initial results a step further by projecting LOS rates onto the landslide itself, comparing them to GPS data, and relating incoherence level to an actual deformation rate, and applying these results to a model of the slide.

Examining the Summer Interferogram Stack

The PBL has been the subject of extensive geotechnical research and monitoring over the past decades. The city of Rancho Palos Verdes collected GPS data starting in 1995, and those data now serve as a means to validate the previously described InSAR observations. There are over 40 GPS stations distributed on and around the PBL, with

campaign observations generally taken every one to three months. The GPS data yield both the displacement rate and direction, which allows for the comparison of LOS observations to deformation on the ground. The GPS benchmarks are densely packed on and around the slide, allowing for accurate resolution of landslide features (Figure 16). Not all benchmarks contain the full time interval of the data, either because high displacement destroyed the benchmarks or because they were installed after data collection began. The GPS data record an average deformation rate in the summer

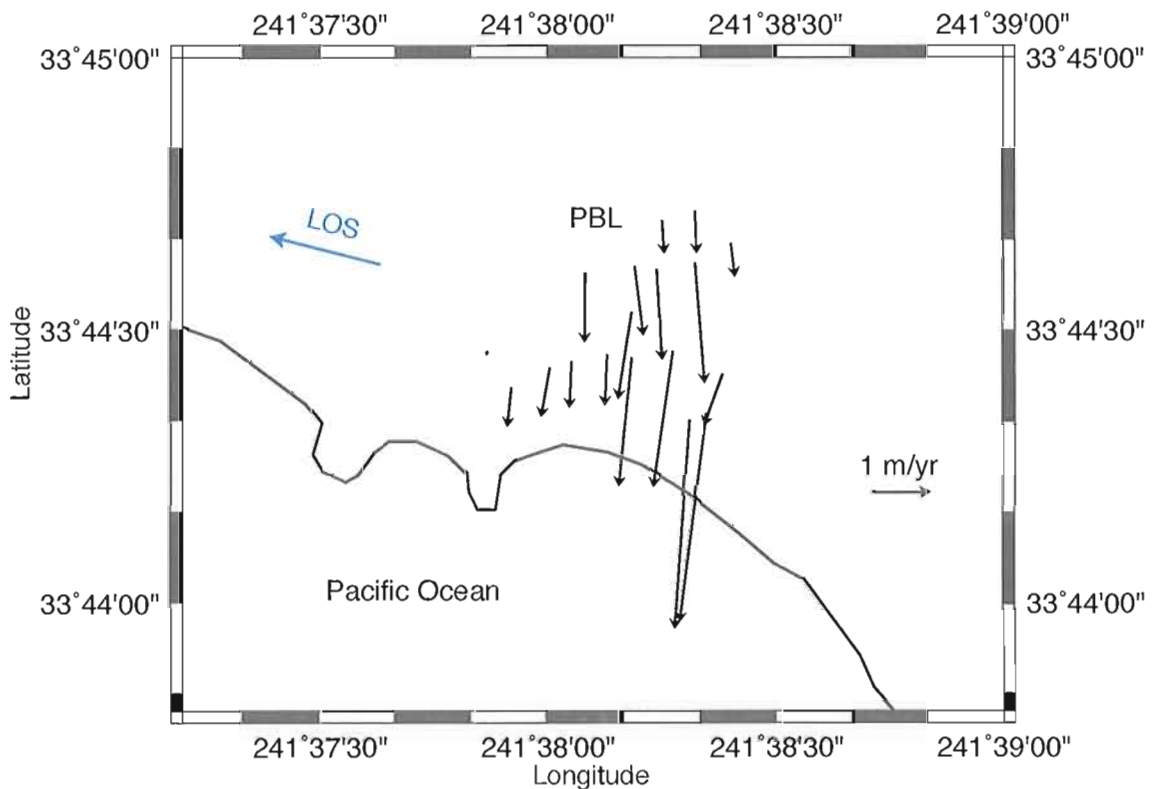


Figure 16. GPS displacements at the PBL. The satellite line-of-sight vector is shown in blue. The directions of the average GPS displacement vector on the PBL and the LOS vector are nearly perpendicular, leaving the satellite blind to much of the horizontal landslide displacement. No uncertainty levels are reported with GPS data set. However, uncertainty for campaign-mode GPS can be as high as several centimeters per year.

months of 1.17 ± 0.28 m/yr. The error reported is one standard deviation from the mean, representing variability in results from different GPS stations across the slide.

The horizontal direction of deformation measured by GPS along with the topographic slope inferred from a DEM is used to calculate three dimensional deformation observed by InSAR. The GPS show displacement vectors that are consistent with a downslope landslide mechanism. Because GPS is less reliable in the vertical direction than the horizontal (*Mao et al.*, 1999), the DEM is used to find the surface dip that describes the vertical component of deformation. The average dip at the landslide is 6.3 degrees, and the average horizontal bearing from GPS is 174.8 degrees west of north. The dip derived from the DEM is consistent with previously measured values (*Ehlig*, 1992).

The LOS vectors (-76.4 degrees E of N for both tracks, 67.0 degrees down and 71.1 degrees down for tracks 170 and 442, respectively) are nearly perpendicular to the direction of horizontal deformation, greatly reducing the signal observed by the satellite. In many cases this is problematic, but for this study it actually helps to resolve the motion. Given a deformation rate of ~ 1 m/yr, it is impossible to unwrap using a SAR wavelength of 5.6 cm if it is parallel to the satellite LOS because several phase cycles would be crossed from one pixel to the next. The satellite, however, is blind to much of the horizontal deformation because its look vector is nearly perpendicular to the displacement vector. This lowers the LOS deformation and prevents phase cycle ambiguities from occurring.

Projecting the deformation direction onto the satellite LOS, the observed deformation rate is a factor of 22.8 larger than the satellite LOS for track 170, and 17.8 times larger for track 442. The scaling factor is found by the following equation:

$$SF = \frac{1}{\hat{l} \cdot \hat{d}} \quad (4)$$

where \hat{l} is the satellite look direction, and \hat{d} is the actual ground deformation direction.

Multiplying the LOS rates by these factors, the summer ground deformation rate for track 170 is 1.04 ± 0.32 m/yr, and 0.97 ± 0.30 m/yr for track 442. The uncertainty reported is one standard deviation from the mean, and it represents the variation in phase for all the pixels across the slide.

Some potential errors are not included in this analysis. Most importantly, spatial variations in dip and bearing across the landslide are ignored. At some points on the slide, dip and bearing combinations may approach angles that are completely perpendicular to the satellite LOS. Thus there is a singularity when \hat{l} and \hat{d} are perpendicular. In practice, however, the observed LOS deformation at these points is zero. Such stationary points, amid others with relatively large phase change, would either become incoherent, get filtered out before interferogram formation, or get averaged with non-zero values in the stacking process. All of these possibilities would effectively smooth out the phase singularity without removing the scaling factor singularity. To avoid these anomalies, the average dip and bearing are used to convert the LOS observations on the displacement vector of the slide.

The InSAR summer displacement rate values are 1.04 ± 0.32 m/yr for track 170 and 0.97 ± 0.30 m/yr for track 442. Combining the two, the average summer displacement rate determined from InSAR observations at the PBL is 1.00 ± 0.31 m/yr, which is within one standard deviation of the GPS deformation rate of 1.17 ± 0.28 m/yr. The GPS data confirm the validity of the InSAR results for the summers between 1995 and 2000.

Temporal Constraints on Decorrelation

The decorrelation mapping described in chapter 3 gives information on the spatial and temporal extent of the PBL. Specifically, the analysis shows that a coherence threshold ($\gamma < 0.4$) is crossed at the end of each fall, resulting in decorrelated patches over the landslide area. Each spring, the patches disappear when γ increases. *Baran et al.* (2005) model the maximum detectable deformation gradient by comparing it to coherence, γ . The maximum deformation gradient is proportional to the length over which the gradient extends, and inversely proportional to temporal baseline (Equation 5).

$$D_{\max} = \frac{\lambda}{2\eta} - \frac{\gamma - 1}{500} \quad (5)$$

where D_{\max} is the maximum detectable LOS deformation rate from one pixel to the next for one epoch, λ is the wavelength, and η is the pixel size. For a coherence threshold of $\gamma=0.4$, $D_{\max}=0.0002$. The length of the deformation gradient and the epoch length are necessary to apply this value to PBL.

I assume that the landslide is described by a rigid block where strain is concentrated along the margins of the block. The actual deformation gradient around the PBL varies significantly along the margins of the slide. The west side of the slide ramps up to high deformation over a very short distance (on the meter scale), while the east side of the slide changes much more gradually (on the 100 meter scale) (*Ehlig*, 1992). An average boundary width of about two pixel widths, or 60 meters, is used in this study. Thus for the shortest possible epoch (35 days), and the width of 60 meters for the margin of the slide, the maximum observable deformation rate is 12.5 cm/yr along the satellite LOS. The LOS rate from summer stack of interferograms (~ 5 cm/yr) is well below this value.

Since the sharp change in decorrelation corresponds to the time when the maximum detectable deformation gradient is exceeded, decorrelation mapping can constrain the time when a pixel exceeds the velocity threshold. Figure 17 shows the decorrelation level over the slide based on all interferograms with epochs less than one year, condensed into a single calendar year as described in chapter 3. A sharp increase in decorrelation occurs between December 1 and January 1. Similarly, a sharp decrease in decorrelation occurs between May 1 and June 1, so the LOS rate drops back below 12.5 cm/yr during that time span. Using the same scaling factors found in equation 4, this LOS rate corresponds to displacement of about 2.5 m/yr.

It is important to note that one does not expect a direct relationship between the amplitudes of rainfall and decorrelation. decorrelation does not measure the deformation rate of the slide directly, and once the slide becomes decorrelated the sliding velocity can

continue to increase with no change in the decorrelation level. Only the steep gradients of the decorrelation are noteworthy.

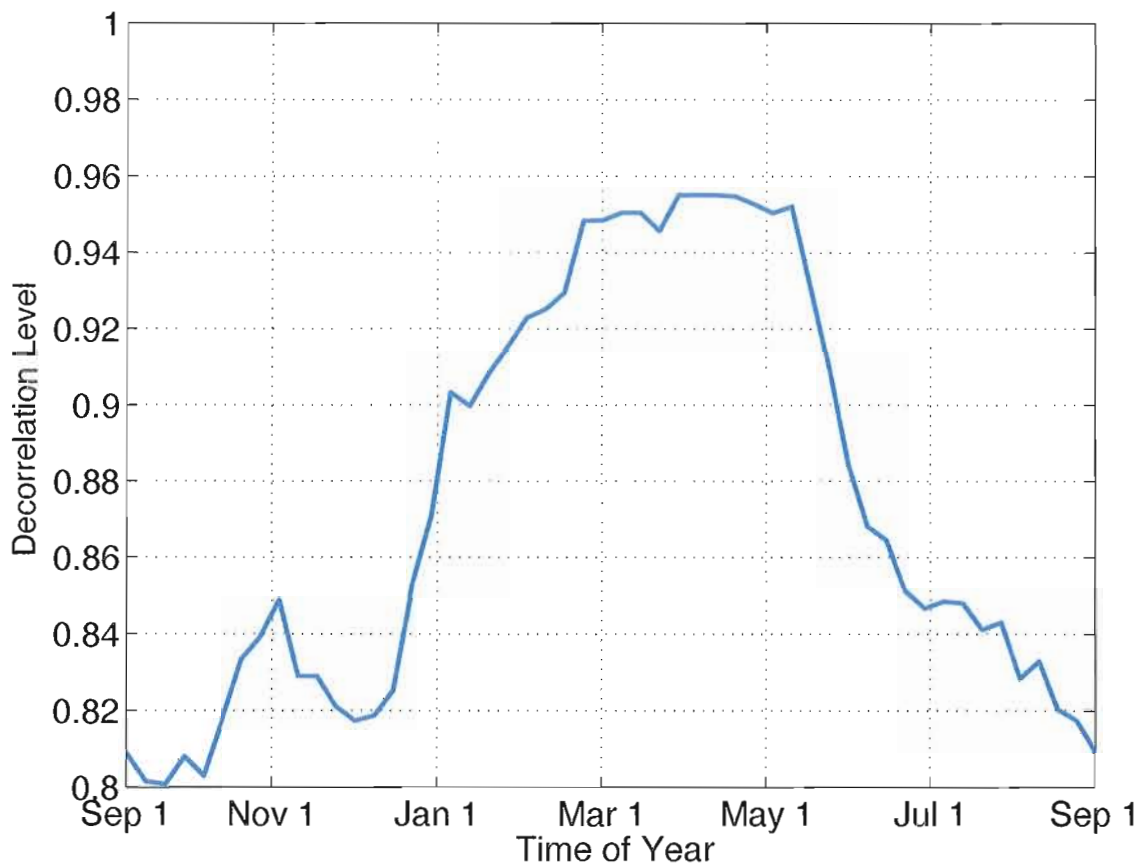


Figure 17. Spatial average of the decorrelation level condensed onto a single calendar year. The sharp gradients in December and May represent times when the maximum detectable deformation gradient corresponding to 2.5 m/yr of displacement is crossed.

The Effect of Rainfall on Decorrelation Level

Previous work shows that the Portuguese Bend landslide is hydrologically driven, with the sliding velocity increasing as the water table rises and pore pressure increases, and decreasing when they fall (Ehlig, 1992). Iverson (2000) describes the relationship between sliding rate and time since rainfall onset. The diffusion of pore pressure through

the slide decreases the normal force and frictional resistance, thereby accelerating the slide. As pore pressure diffuses through the slide there is a lag between the onset of rainfall and the acceleration of the slide. Rain gauge data collected by the city of Palos Verdes city can be combined with the incoherence level to measure how long it takes after the rainy season begins for the slide to cross the coherence threshold.

Rain gauge data is analyzed to determine the when the rainy season begins (Figure 18). To quantify the date of rainfall onset, a threshold of 0.75 inches cumulative rainfall during the water year is set. The water year begins October 1 each year, while precipitation is still at the extremely low summer level. Examining the data, only trace amounts of rain fall each water year before crossing this threshold, and once cumulative rainfall does exceed 0.75 inches, it tends to continue raining consistently. Averaging rain gauge data from October 1995 to October 1999 yields a rainfall initiation date of November 15, plus or minus two weeks. With the displacement quantified by the crossing of the coherence threshold (2.5 m/yr) confined to between December 1 and January 1, the lag time between the onset of rainfall and this displacement is about one month (Figure 19).

While it would be useful to compare a full time series of the decorrelation level to the rainfall from 1995 to 2000, the temporal resolution of the decorrelation level is too low to retrieve lag times. As described in chapter 3, new data is theoretically acquired twice every 35 days. In practice, however, interferograms are not produced for every possible SAR pair, so the InSAR results are coarsely sampled relative to the rainfall.

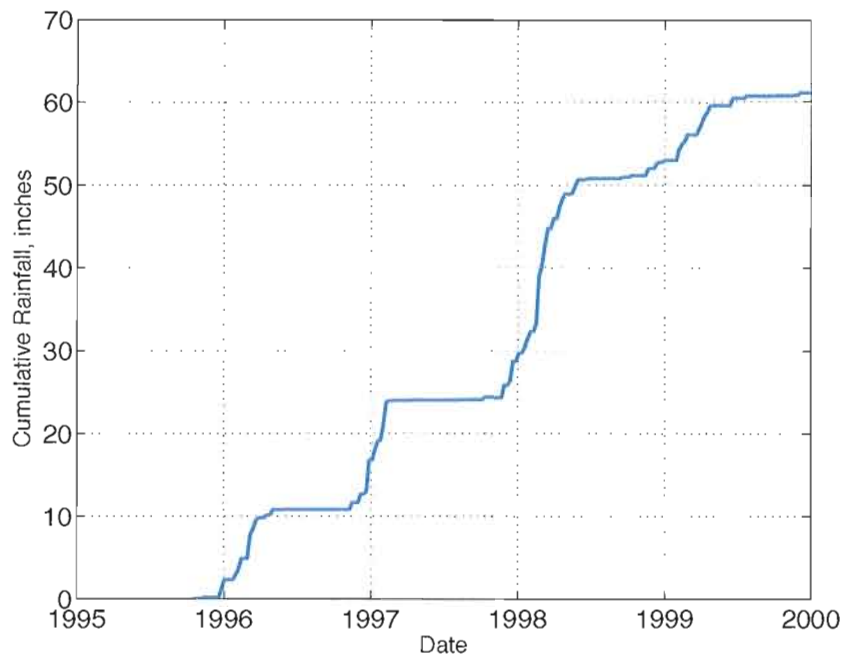


Figure 18. Cumulative rainfall at the Portuguese Bend, beginning October 1, 1995. The rainy season begins when 0.75 inches have fallen during the water year.

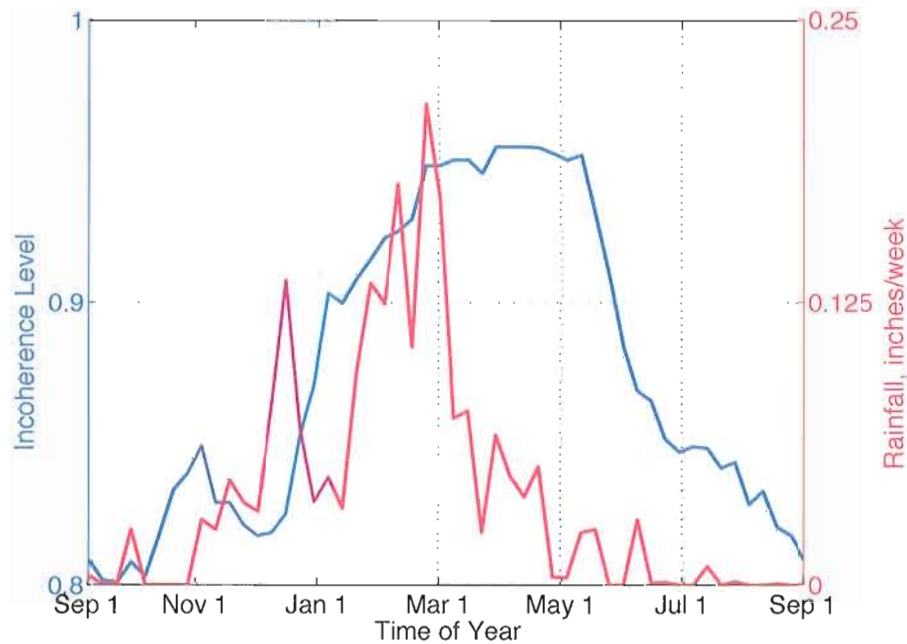


Figure 19. Average decorrelation level with average rainfall in blue and red, respectively. The red and blue bars indicate the onset of rainfall and initiation of fast deformation, respectively. The lag between the two is about one month.

Modeling for Hydraulic Diffusivity

Iverson's (2000) model predicts a relationship between landslide velocity and time lag following a rainfall event. It describes how pore pressure diffuses through a landslide on different time scales. The rainwater increases pore pressure, which sends pressure waves through the sliding mass, reducing friction at the base of the slide and initiating movement. Here the model is evaluated as one potential application of the results obtained from the InSAR data. Figure 20 is reproduced from Iverson's paper, and it shows both the theoretical and experimental relationship between v and t for parameters at the Minor Creek slide in northern California. Both the Minor Creek and the Portuguese Bend landslides are hydrologically driven and slow moving, allowing a valid comparison between the two. The following is the relationship Iverson derives to govern his model:

$$\frac{dv^*}{dt^*} = S \sin \alpha [1 - FS_0(Z)] + S \frac{\gamma_w \tan \phi}{\gamma_s \cos \alpha} \frac{I_Z}{K_Z} \cdot \begin{cases} [R(t^*)] & t^* \leq T^* \\ [R(t^*) - R(t^* - T^*)] & t^* > T^* \end{cases}, \quad (6)$$

On the left-hand side is the derivative of the normalized velocity, v^* , with respect to normalized time, t^* . The velocity has been normalized so that $v^* = v/(Zg)^{0.5}$, where Z is the depth of the slide and g is gravity. On the right-hand side of the equation there are two terms. The first includes the factor of safety (FS), which is set to 1 for the point at which slope failure occurs. The remainder of the equation is a function of the normalized time, t^* , where $t^* = (4 D_o t \cos^2 \alpha)/Z^2$. D_o , the diffusivity, is the variable I ultimately wish to determine. The leading coefficients are properties of the landslide: γ_s is soil unit weight, γ_w is pore water unit weight, α is slope angle, ϕ is friction angle, S is a scaling coefficient.

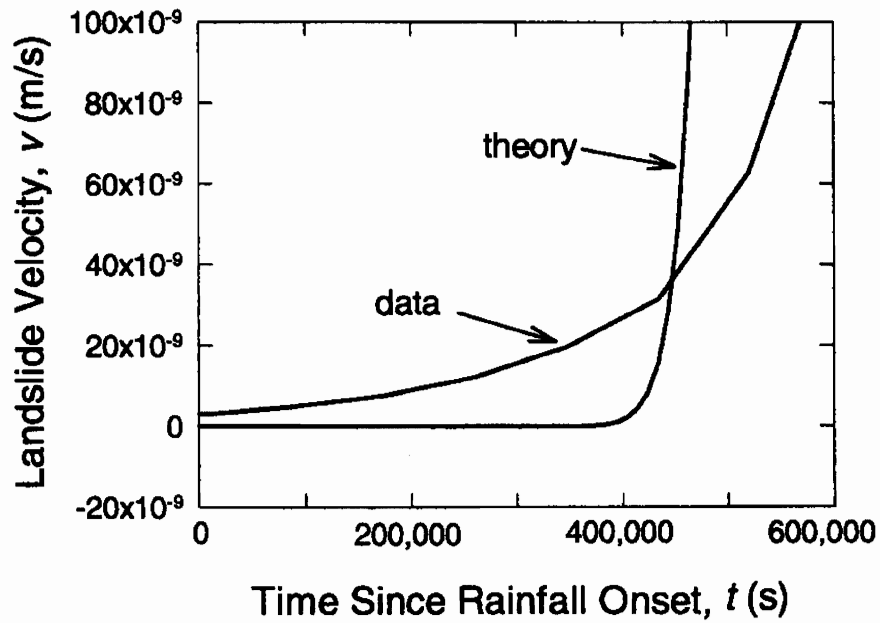


Figure 20. Landslide velocity as a response to lag time. Reproduced from *Iverson* (2000). This plot shows the relationship between time since rainfall onset and landslide velocity for the Minor Creek landslide in northern California.

and I_z/K_z is the normalized infiltration rate (Table 2). The normalized time, t^* , appears in the form of Richard's equation, as shown below:

$$R(t^*) = \sqrt{t^*/\pi} \exp(-1/t^*) - \operatorname{erfc}(1/\sqrt{t^*}) \quad (7)$$

Iverson uses known parameters from Minor Creek to predict the landslide velocity at certain times. The decorrelation analysis presented earlier in the chapter yields the landslide velocity at one specific time, the time since the onset of rainfall. Fitting the model to the data, I am therefore able to estimate for a specific parameter of interest, D_o . Diffusivity plays a vital role in slide mechanics, dictating how quickly pore pressure moves through the slide. The unknown parameters in equation 6 are the normalized vertical infiltration rate, I_z/K_z , and the diffusivity, D_o . Because the modeled velocity is

Parameter	Variable	Value at the PBL
Slope angle	α	6.3°
Landslide depth	Z	18 m
Friction angle	ϕ	6°
Soil unit weight, wet	γ_s	22000 N/m ³

Table 2. Landslide parameters at the PBL used to solve equation 6.

much more sensitive to diffusivity than infiltration rate, I can constrain D_o for the full range of realistic values of I_z/K_z (Iverson, 2000).

Integrating equation 6 yields the velocity, v^* , with respect to the time since rainfall onset, t^* (Figure 21). The two red points are the summer displacement rate and the high displacement corresponding to the maximum detectable deformation gradient. Reasonable values of I_z/K_z are between 0.1 and 5, so the vertical infiltration rate is between one tenth and five times the vertical hydraulic conductivity. For a given D_o , varying I_z/K_z between 0.1 and 5 creates the family of curves shown on each plot. The value of D_o that fits for the most extreme case of I_z/K_z is used to constrain D_o . Higher values of I_z/K_z push the curve to the left, lower values push it to the right. In figure 21, the upper panel corresponds to $D_o = 1.40 \times 10^{-6} \text{ m}^2/\text{s}$, and lower to $D_o = 1.65 \times 10^{-6} \text{ m}^2/\text{s}$. Even without constraining I_z/K_z , the model constrains D_o to this narrow band of values.

The time lag between onset of rainfall and fast displacement corresponding to the maximum detectable deformation gradient is only a rough estimate. In addition to setting the lag to four weeks, I also find D_o given 50% error in the value, allowing the lag time to range from two to six weeks (Figure 22). I_z/K_z is still allowed to vary through all

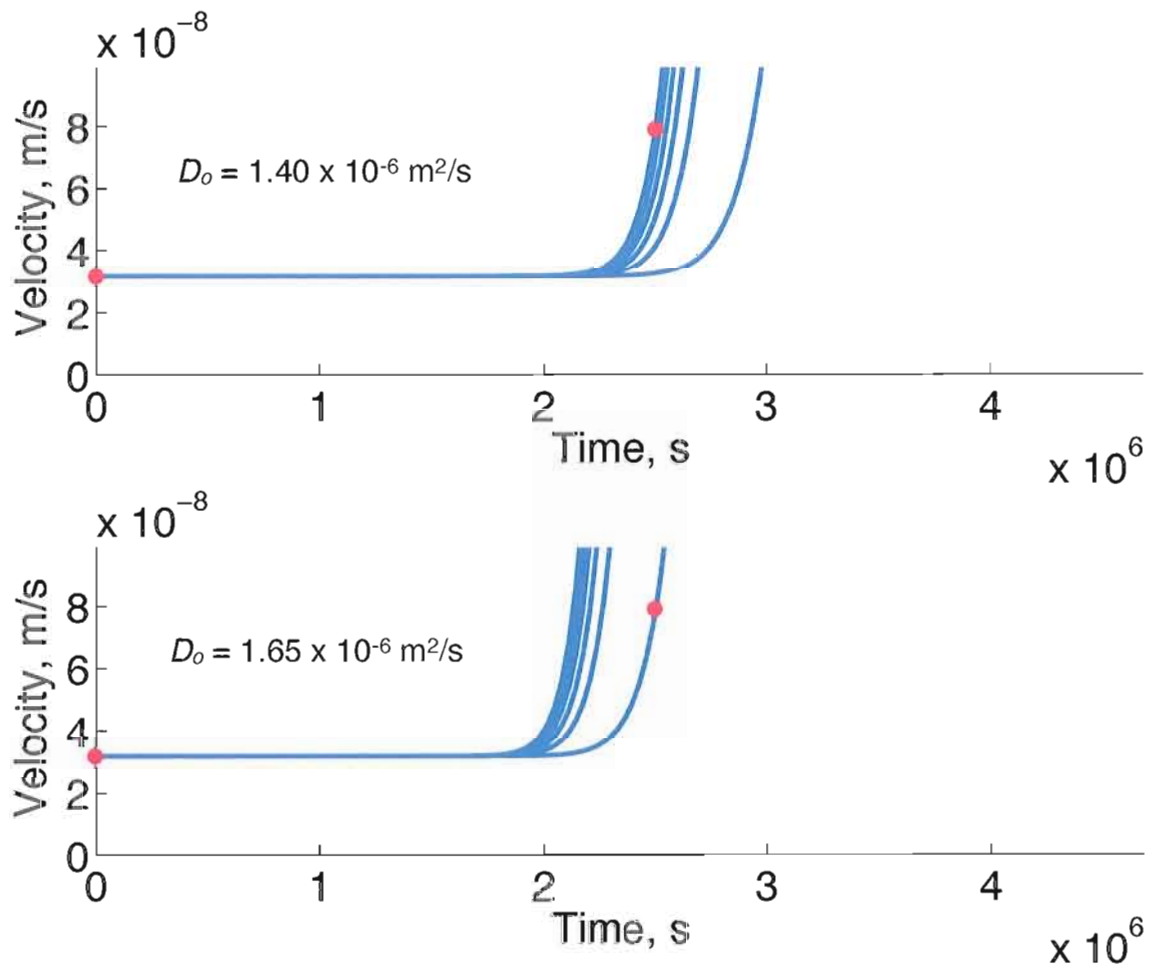


Figure 21. Modeling results using a four week lag time. Velocity and time plotted for I_z/K_z values ranging from 0.1 to 5 (from the right to the left) and two D_o values, $1.40 \times 10^{-6} \text{ m}^2/\text{s}$ on the left panel and $1.65 \times 10^{-6} \text{ m}^2/\text{s}$ on the right panel. Even the wide variation in I_z/K_z has little effect of D_o .

reasonable values. This method now puts the outer bounds for diffusivity at $0.9 \times 10^{-6} \text{ m}^2/\text{s}$ in the upper panel, and $3.5 \times 10^{-6} \text{ m}^2/\text{s}$ in the lower panel. Iverson finds $D_o = 1 \times 10^{-6}$ at the Minor Creek landslide, similar to the value found for the PBL. This makes sense given that the landslides are both slow-moving, hydrologically driven slides.

Hilley et al. (2004) report a lag time between the beginning of the rainy season and the sharp increase in sliding velocity at the Berkeley Hills of up to ~ 3 months. At

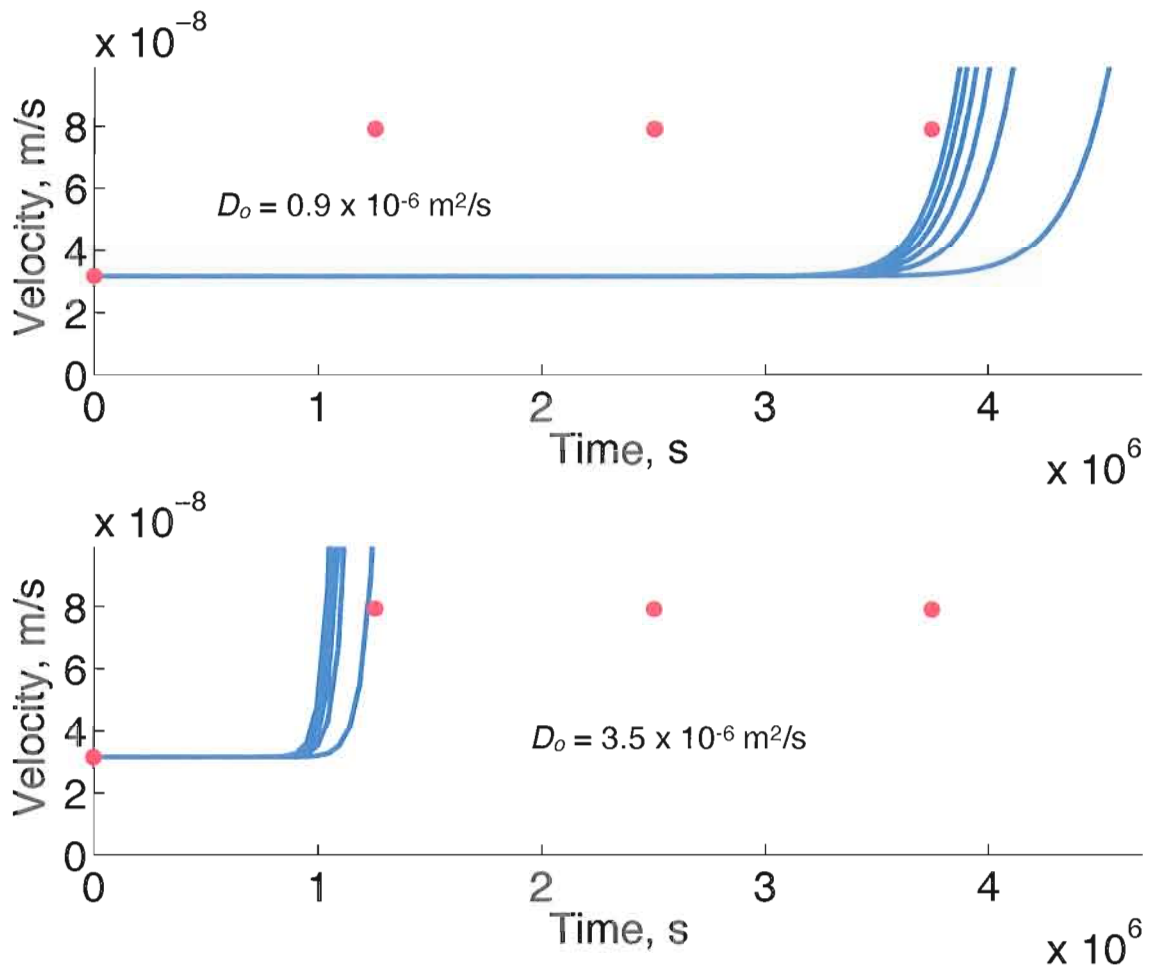


Figure 22. Modeling results using a two to six week lag time. Velocity and time plotted for I_z/K_z values ranging from 0.1 to 5 (from the right to the left) and two D_o values, $0.9 \times 10^{-6} \text{ m}^2/\text{s}$ on the left panel and $3.5 \times 10^{-6} \text{ m}^2/\text{s}$ on the right panel. The red dots show three different possible time lags, two, four, and six weeks.

Minor Creek, *Iverson* (2000) finds a lag time of 5-8 days. Through InSAR observations, I estimate the lag time at the PBL to be 2-6 weeks. These three landslides are hydrologically similar, each characterized by slow, non-catastrophic movement. However, they have very different responses to rainfall. Examining the landslide parameters, landslide depth appears to be a determining factor in this response. Rainfall that percolates into the ground initiates a pressure wave that travels through the saturated

sliding mass, eventually decreasing the frictional resistance at the sliding boundary.

Therefore, a deeper landslide is expected to have a more delayed response to rainfall. The depth of the Minor Creek landslide is about 6 meters and it has the shortest lag time (*Iverson, 2000*). The average depth at the PBL is 18 meters (*Vonder Linden, 1989*), and it has an intermediate lag time. The Berkeley Hills have the longest lag time and the greatest depth, at about 30 meters (*Hilley et al., 2004*).

CHAPTER V

SUMMARY AND CONCLUSIONS

This study of the Portuguese Bend landslide has incorporated several different remote sensing methods in an attempt to monitor the slide, better understand its dynamics, and constrain important physical parameters. First, conventional satellite interferometry is used to determine the deformation rate during the summer months when the rate is relatively low. The ground deformation rate is found to average 1.00 ± 0.31 m/yr along a down-slope unit vector. Next, decorrelated patches over many interferograms are combined to constrain the spatial and temporal extent of the slide. A maximum detectable deformation gradient is reached when the phase gradient reaches a value of 2π radians per pixel. A deformation rate is implied by this gradient when applied to the parameters of the slide. This rate of 2.5 m/yr is confined to the months of December and May. Finally, I find that a diffusivity value of 0.9×10^{-6} to 3.5×10^{-6} m²/s is required to explain the lag time between rainfall onset and acceleration of the slide.

The summer deformation rate of 1.00 ± 0.31 m/yr falls within one standard deviation of the rate measured by the GPS network, 1.17 ± 0.28 m/yr. While individual several-month to year-long interferograms are not necessarily coherent over the landslide, enough short time-span interferograms during the summer months are coherent to obtain

an average deformation rate for the same time period. This result is encouraging for the InSAR and geomorphology communities, showing that stacking many short-duration interferograms can extract a signal from a noisy data set.

Although phase decorrelation is often ignored in InSAR studies, it actually yields important information about the PBL. By mapping decorrelation through time, the spatial boundaries of the landslide are estimated and agree with the boundaries mapped in the field. Additionally, the timing of when the slide accelerates to velocities greater than 2.5 m/yr, as characterized by the steep phase gradient along the edges of the slide, is confined between the months of December and May. Combining this result with rain gauge data, the lag time between the onset of rainfall and the acceleration of the slide is determined to be about one month. Mapping phase decorrelation requires a larger data set than the stacking techniques used for coherent summer interferograms. If enough scenes are collected, however, this method can be used to track the evolution of events (such as landslides) where the deformation rate is too fast to unwrap properly.

The increased decorrelation level in the winter demonstrates that the landslide moves faster in the winter than the summer, consistent with previous studies that suggest that the slide is hydrologically driven. During the summer months the water table drops, reducing the pore pressure at the base of the slide, increasing frictional resistance, and decreasing slide velocity in response. Once rainfall re-initiates in the fall, there is about a 2-6 week lag time during which the rainwater generates pore pressure waves that percolate down through the slide, reducing frictional resistance and increasing sliding velocity. Applying the Iverson (2000) landslide dynamics model to the PBL, I find D_o to

be between 0.9×10^{-6} and 3.5×10^{-6} m²/s, despite the large error in the lag time. This diffusivity is similar to or slightly higher than that of the Minor Creek landslide, which *Iverson* (1987) examines in detail. Comparing physical parameters at the PBL to those determined at Minor Creek (*Iverson*, 2000) and the Berkeley Hills (*Hilley et al.*, 2004), I find that the PBL has both an intermediate lag time and landslide depth. The lag time is 2-6 weeks, as compared to 5-8 days at Minor Creek and ~3 months at the Berkeley hills, and the landslide depth is 18 meters, compared to 6 meters at Minor Creek and 30 meters at the Berkeley Hills. This suggests that for landslides with similar hydrologic properties, depth is a primary factor in determining the slide's response to rainfall.

All the techniques demonstrated here would be improved by implementing a shorter satellite repeat cycle. Even slow-moving, non-catastrophic landslides such as the Portuguese Bend often deform too quickly to be examined using a satellite with a 35-day repeat cycle. With a shorter cycle, the phase gradient unwrapping threshold would be less likely to be exceeded (see equation 4), and a larger number of coherent interferograms could be formed. Even if that threshold were still crossed for part of the year, decorrelation mapping would yield data with higher temporal resolution, allowing tighter constraints on when the unwrapping threshold is crossed. The coherent summer stacking technique only works for landslides with LOS deformation rates below the phase unwrapping threshold, and incoherence mapping works only for slides which are below the threshold for part of the year and above the threshold for the rest. Landslides that do not drop below the unwrapping threshold can be confined spatially with decorrelation mapping, and changes in slide area can be monitored, but no velocity information would

be determined with these techniques. L-band ALOS data will prove more effective for imaging the slide given its longer wavelength signal. This will increase the maximum unwrappable deformation rate determined in equation 4, perhaps enough to make winter interferograms coherent.

One simple step to further this study would be to extend the date range of the data from 2000 up to the present. Little work has been published on the landslide since Ehlig's major overview in 1992 despite the fact that GPS data exists. *Kayen et al.* (2002) describe deformation through the 1990's qualitatively, but most other work has been confined to the private sector. InSAR would be a relatively inexpensive way to monitor the PBL and check the progress of mitigation attempts. Although few studies have focused on the PBL recently, there is a long history of previous work, making it an attractive site to attempt new monitoring techniques. Although the methods here are limited in applicability by deformation rate, satellite repeat rate, and wavelength, they may prove useful in future landslide studies.

APPENDIX A
TABLE OF SAR SCENES USED

Satellite	Track	Frame	Orbit	Date
ERS1	170	2925	4824	19920617
ERS1	170	2925	5826	19920826
ERS1	170	2925	6327	19920930
ERS1	170	2925	7830	19930113
ERS1	170	2925	10335	19930707
ERS1	170	2925	11337	19930915
ERS1	170	2925	11838	19931020
ERS1	170	2925	12339	19931124
ERS1	170	2925	19697	19950421
ERS1	170	2925	20198	19950526
ERS1	170	2925	20699	19950630
ERS1	170	2925	21200	19950804
ERS1	170	2925	21701	19950908
ERS1	170	2925	22202	19951013
ERS1	170	2925	22703	19951117
ERS1	170	2925	23204	19951222
ERS1	170	2925	23705	19960126
ERS1	170	2925	24707	19960405
ERS1	170	2925	25208	19960510
ERS2	170	2925	2529	19951014
ERS2	170	2925	3030	19951118
ERS2	170	2925	3531	19951223
ERS2	170	2925	4032	19960127
ERS2	170	2925	5034	19960406
ERS2	170	2925	5535	19960511
ERS2	170	2925	6036	19960615
ERS2	170	2925	7038	19960824
ERS2	170	2925	7539	19960928
ERS2	170	2925	8040	19961102
ERS2	170	2925	8541	19961207
ERS2	170	2925	9042	19970111
ERS2	170	2925	10545	19970426
ERS2	170	2925	11046	19970531
ERS2	170	2925	11547	19970705
ERS2	170	2925	12048	19970809
ERS2	170	2925	12549	19970913
ERS2	170	2925	13050	19971018
ERS2	170	2925	13551	19971122
ERS2	170	2925	14052	19971227
ERS2	170	2925	14553	19980131
ERS2	170	2925	15054	19980307
ERS2	170	2925	15555	19980411

Satellite	Track	Frame	Orbit	Date
ERS2	170	2925	16056	19980516
ERS2	170	2925	16557	19980620
ERS2	170	2925	17058	19980725
ERS2	170	2925	17559	19980829
ERS2	170	2925	18060	19981003
ERS2	170	2925	18561	19981107
ERS2	170	2925	19062	19981212
ERS2	170	2925	19563	19990116
ERS2	170	2925	20064	19990220
ERS2	170	2925	21066	19990501
ERS2	170	2925	21567	19990605
ERS2	170	2925	22068	19990710
ERS2	170	2925	22569	19990814
ERS2	170	2925	23571	19991023
ERS2	170	2925	24072	19991127
ERS2	170	2925	25074	20000205
ERS2	170	2925	25575	20000311
ERS2	170	2925	26076	20000415
ERS2	170	2925	26577	20000520
ERS2	170	2925	27078	20000624
ERS2	170	2925	27579	20000729
ERS2	170	2925	28080	20000902
ERS2	170	2925	29082	20001111
ERS2	170	2925	29583	20001216
ERS2	170	2925	30585	20010224
ERS2	170	2925	32589	20010714
ERS2	170	2925	33090	20010818
ERS2	170	2925	33591	20010922
ERS2	170	2925	34092	20011027
ERS2	170	2925	34593	20011201
ERS2	170	2925	35094	20020105
ERS2	170	2925	36597	20020420
ERS2	170	2925	38100	20020803
ERS1	442	2925	4595	19920601
ERS1	442	2925	6098	19920914
ERS1	442	2925	6599	19921019
ERS1	442	2925	7100	19921123
ERS1	442	2925	7601	19921228
ERS1	442	2925	8603	19930308
ERS1	442	2925	11108	19930830
ERS1	442	2925	11609	19931004
ERS1	442	2925	12110	19931108

Satellite	Track	Frame	Orbit	Date
ERS1	442	2925	19468	19950405
ERS1	442	2925	19969	19950510
ERS1	442	2925	20470	19950614
ERS1	442	2925	20971	19950719
ERS1	442	2925	21472	19950823
ERS1	442	2925	21973	19950927
ERS1	442	2925	22474	19951101
ERS1	442	2925	22975	19951206
ERS1	442	2925	23476	19960110
ERS1	442	2925	23977	19960214
ERS1	442	2925	24979	19960424
ERS1	442	2925	25480	19960529
ERS2	442	2925	2801	19951102
ERS2	442	2925	3302	19951207
ERS2	442	2925	3803	19960111
ERS2	442	2925	4304	19960215
ERS2	442	2925	5306	19960425
ERS2	442	2925	6308	19960704
ERS2	442	2925	7310	19960912
ERS2	442	2925	7811	19961017
ERS2	442	2925	8312	19961121
ERS2	442	2925	8813	19961226
ERS2	442	2925	9815	19970306
ERS2	442	2925	10316	19970410

Satellite	Track	Frame	Orbit	Date
ERS2	442	2925	10817	19970515
ERS2	442	2925	11318	19970619
ERS2	442	2925	11819	19970724
ERS2	442	2925	12320	19970828
ERS2	442	2925	13322	19971106
ERS2	442	2925	13823	19971211
ERS2	442	2925	14324	19980115
ERS2	442	2925	14825	19980219
ERS2	442	2925	15827	19980430
ERS2	442	2925	17330	19980813
ERS2	442	2925	17831	19980917
ERS2	442	2925	18332	19981022
ERS2	442	2925	18833	19981126
ERS2	442	2925	19334	19981231
ERS2	442	2925	19835	19990204
ERS2	442	2925	20336	19990311
ERS2	442	2925	22340	19990729
ERS2	442	2925	23342	19991007
ERS2	442	2925	23843	19991111
ERS2	442	2925	24344	19991216
ERS2	442	2925	26348	20000504
ERS2	442	2925	26849	20000608
ERS2	442	2925	27851	20000817
ERS2	442	2925	29354	20001130

APPENDIX B
SCENE INDEX FOR PS SERIES

Track 170, 1995-1997
Oct 13, 1995
Nov 17, 1995
Nov 18, 1995
Dec 23, 1995
Jan 27, 1996
Apr 5, 1996
<i>Apr 6, 1996</i>
May 11, 1996
Jun 15, 1996
Sep 28, 1996
Nov 2, 1996
Dec 7, 1996
Jan 11, 1997
Apr 26, 1997
Sep 13, 1997

Track 170, 1997-2000
Sep 13, 1997
Oct 18, 1997
Nov 22, 1997
Jan 31, 1998
Apr 11, 1998
Jul 25, 1998
Aug 29, 1998
Jan 16, 1999
<i>May 1, 1999</i>
Jul 10, 1999
Oct 23, 1999
Nov 27, 1999
Feb 5, 2000
Mar 11, 2000
Apr 15, 2000

Track 442, 1995-1997
Apr 5, 1995
May 10, 1995
Sep 27, 1995
Nov 2, 1995
Dec 7, 1995
Jan 11, 1996
Feb 14, 1996
Feb 15, 1996
Apr 24, 1996
Apr 25, 1996
Jul 24, 1996
<i>Sep 12, 1996</i>
Nov 21, 1996
Dec 26, 1996
Mar 6, 1997
Apr 10, 1997
May 15, 1997
Jun 19, 1997
Jul 24, 1997

Track 442, 1997-2000
Mar 6, 1997
May 15, 1997
Jun 19, 1997
Jul 24, 1997
Jan 15, 1998
Feb 19, 1998
Apr 30, 1998
Aug 13, 1998
Oct 22, 1998
<i>Nov 26, 1998</i>
Feb 4, 1999
Mar 11, 1999
Oct 7, 1999
May 4, 2000
Jun 8, 2000
Aug 17, 2000
Nov 30, 2000

Italics represent master scene for each series.

REFERENCES

- Baran, I., M. Stewart, and S. Claessens, 2005. A New Functional Model for Determining Minimum and Maximum Detectable Deformation Gradient Resolved by Satellite Radar Interferometry. *IEEE Transactions on Geoscience and Remote Sensing*, **43** (4): 675-682.
- Bawden, G. W., W. Thatcher, and R. S. Stein, 2001. Tectonic contraction across Los Angeles after removal of groundwater pumping effects. *Nature*, **412** (6849): 812-815.
- Brooks, B. A., M. A. Merrifield, and J. Foster, 2007. Space geodetic determination of spatial variability in relative sea level change, Los Angeles basin. *Geophysical Research Letters*, **34** (1): L01611.
- Bryant, M. E., 1982. Geomorphology, neotectonics, and ages of marine terraces, Pales Verdes Peninsula. Cooper, J. D., compiler, Landslides and landslide mitigation in southern California, *Association of Engineering Geologists, southern California Section*, p. 15-25.
- Bürgmann, R., P. A. Rosen, and E. J. Fielding, 2000. Synthetic Aperture Radar Interferometry to Measure Earth's Surface Topography and Its Deformation. *Annual Reviews of Earth Planetary Science*, **28**: 169-209.
- Carnec, C., D. Massonnet, and C. King, 1996. Two examples of the use of SAR interferometry on displacement fields of small spatial extent. *Geophysical Research Letters*, **23** (24): 3579-3582.
- Catani, F., P. Farina, S. Moretti, G. Nico, and T. Strozzi, 2005. On the application of SAR interferometry to geomorphological studies: Estimation of landform attributes and mass movements. *Geomorphology*, **66** (1-4): 119-131.
- Colesanti, C., A. Ferretti, F. Novali, C. Prati, and F. Rocca, 2003a. SAR Monitoring of Progressive and Seasonal Ground Deformation Using the Permanent Scatterers Technique, *IEEE Transactions on Geoscience and Remote Sensing*. **41** (7): 1685-1701.

- Colesanti, C., A. Ferretti, C. Prati, and F. Rocca, 2003b. Monitoring landslides and tectonic motions with the permanent scatterers Technique. *Engineering Geology*, **68**: 3-14.
- Ehlig, P. L., 1982. Mechanics of the Abalone Cove landslide including the role of groundwater in landslide stability and a model for development of large landslides in the Pales Verdes Hills. Cooper, J. D., compiler, Landslides and landslide mitigation in southern California, *Association of Engineering Geologists, Southern California Section*, p. 57-66.
- Ehlig, P. L., 1986. The Portuguese Bend landslide; Its mechanics and a plan for its stabilization. Ehlig, P. L., compiler, Landslides and landslide mitigation in southern California, Guidebook and volume prepared for 82nd meeting of Cordilleran Section, *Geological Society of America*, p. 167-172.
- Ehlig, P. L., 1992. Evolution, mechanics and mitigation of the Portuguese Bend landslide, Palos Verdes Peninsula, California. Special Publication, *Association of Engineering Geologists*, **4**: 531-553.
- Emery, K. O., 1967. The activity of coastal landslides related to sea level. *Revue de Géographie Physique et de Géologie Dynamique*, **9**: 177-180.
- Farina, P., D. Colombo, A. Fumagalli, F. Marks, and S. Moretti, 2006. Permanent Scatterers for landslide investigations: outcomes from the ERS-SLAM project. *Engineering Geology*, **88**: 200-217.
- Ferretti, A., C. Prati, and F. Rocca, 2001. Permanent Scatterers in SAR Interferometry. *IEEE Transactions on Geoscience and Remote Sensing*, **39** (1): 8-20.
- Ferretti, A., A. Prati, F. Rocca, N. Casagli, P. Farina, and B. Young, 2003. Permanent Scatterers technology: a powerful state of the art tool for historic and future monitoring of landslides and other terrain instability phenomena. *Proc. of 2005 International Conference on Landslide Risk Management*, A. A. Balkema, Vancouver, Canada, CD-Rom.
- Finnegan, N. J., M. E. Pritchard, R. B. Lohman, and P. R. Lundgren, 2008. Constraints on surface deformation in the Seattle, WA, urban corridor from satellite radar interferometry time-series analysis. *Geophysics Journal International*, **174**: 29-41.

- Fruneau, B., J. Achache, and C. Delacourt, 1996. Observation and modeling of the Saint-Étienne-de-Tinée landslide using SAR interferometry. *Tectonophysics*, **265**: 181-190.
- Furuya, M., K. Mueller and J. Wahr, 2007. Active salt tectonics in the Needles District, Canyonlands (Utah) as detected by interferometric synthetic aperture radar and point target analysis: 1992-2002. *Journal of Geophysical Research*, **112** (B6): B06418 .
- Gabet, E., and T. Dunne, 2002. Landslides on coastal sage-scrub and grassland hillslopes in a severe El Niño winter: The effects of vegetation conversion on sediment delivery. *GSA Bulletin*, **114** (8): 983-990.
- Hanssen, R., T. Weckwerth, H. Zebker and R. Klees, 1999. High-resolution water vapor mapping from interferometric radar measurements,. *Science*, **283**: 1297–1299.
- Hanssen, R. F., 2001. *Radar Interferometry: Data Interpretation and Error Analysis*. Springer, New York.
- Hill, C., 2000. A geochemical and hydrological assessment of groundwater in the Portuguese Bend landslide, California. Ph.D. Dissertation, University of Southern California, Los Angeles.
- Hilley, G. E., R. Burgmann, A. Ferretti, F. Novali, and F. Rocca, 2004. Dynamics of slow-moving landslides from permanent scatterer analysis. *Science*, **304**: 1952-1955.
- Hooper, A., 2006. Persistent Scatterer Radar Interferometry for Crustal Deformation Studies and Modeling of Volcanic Deformation. Ph.D. Dissertation, Stanford University, Palo Alto.
- Hooper, A., P. Segall, and H. Zebker, 2007. Persistent scatterer interferometric synthetic aperture radar for crustal deformation analysis, with application to Volcán Alcedo, Galápagos. *Journal of Geophysical Research*, **112**: B07407.
- Iverson, R. M., and J. J. Major, 1987. Rainfall, ground-water flow, and seasonal movement at Minor Creek landslide, northwestern California: Physical interpretation of empirical relations. *Geological Society of America Bulletin*, **99**, 579-594.
- Iverson, R. M., 2000. Landslide triggering by rain infiltration. *Water Resources Journal*, **207**: 59-82.

- Jennings, C.W., 1994. Fault Activity Map of California and Adjacent Areas. Geologic Data Map No. 6, scale 1:750,000. California Div. Mines & Geology, Sacramento.
- Kayen, R. E., 2002. Influence of the Portuguese Bend landslide on the character of the effluent-affected sediment deposit, Palos Verdes margin, Southern California. *Continental Shelf Research*, **22**: 911-922.
- Kew, W. S., 1926. Geologic and physiographic features in the San Pedro Hills, Los Angeles County, California. *Oil Bulletin*, **12**: 513-518.
- Kimura, H., and Y. Yamaguchi, 2000. Detection of Landslide Areas Using Satellite Radar Interferometry. *Photogrammetric Engineering & Remote Sensing*, **66** (3): 337-344.
- Lanari, R. P. Lundgren, and M. Manzo, 2004. Satellite radar interferometry time series analysis of surface deformation for Los Angeles, California. *Geophysical Research Letters*, **31** (23), L23613.
- Li, Z., J. Muller, P. Cross, and E. J. Fielding, 2005. Interferometric synthetic aperture radar (InSAR) atmospheric correction: GPS, Moderate Resolution Imaging Spectroradiometer (MODIS), and InSAR integration. *Journal of Geophysical Research*, **110**: B03410.
- Mao, A., C. G. A. Harrison, and T. H. Dixon, 1999. Noise in GPS coordinate time series. *Journal of Geophysical Research*, **104** (B2), 2797-2816.
- Merriam, R., 1960. Portuguese Bend landslide, Pales Verdes Hills, California. *Journal of Geology*, **68**: 140-153.
- Munz, P. A., 1979. *A Flora of Southern California*. University of California Press, Berkeley.
- Price, E. J., and D. T. Sandwell, 1998. Small-scale deformations associated with the 1992 Landers, California, earthquake mapped by synthetic aperture radar interferometry phase gradients. *Journal of Geophysical Research*, 98JB01821.
- Rosen, P. A., S. Hensley, G. Peltzer, and M. Simons, 2004. Updated repeat orbit interferometry package released. *EOS Transactions AGU*, **85** (5): 47.

- Salvi, S., S. Atzori, C. Tolomei, J. Allievi, A. Ferretti, F. Rocca, C. Prati, S. Stramondo, and N. Feuillet, 2004. Inflation rate of the Colli Albani volcanic complex retrieved by the permanent scatterers SAR interferometry technique. *Geophysical Research Letters*, **31**: L12606.
- Squarzoni, C., C. Delacourt, and P. Allemand, 2003. Nine years of spatial and temporal evolution of the La Valette landslide observed by SAR interferometry. *Engineering Geology*, **68** (1-2): 53-66.
- Terzaghi, K., 1950. Mechanics of landslides. *Application of Geology to Engineering Practice*, p. 83-123.
- Vonder Linden, K., 1972. An analysis of the Portuguese Bend landslide, Palos Verdes Hills, California. Ph.D. Dissertation, Stanford University.
- Vonder Linden, K., 1989. The Portuguese Bend Landslide. *Engineering Geology*, **27**: 301-373.
- Watson, K. M. Y. Bock, and D. T. Sandwell, 2002. Satellite interferometric observations of displacements associated with seasonal groundwater in the Los Angeles basin. *Journal of Geophysical Research-Solid Earth*, **107** (B4): 2074.
- Woodring, W. P., M. N. Bramlette, and W. S. W. Kew, 1946. Geology and paleontology of the Palos Verdes Hills, California. *U.S. Geological Survey Professional Paper 207*. Washington, D.C.: U.S. Government Printing Office.
- Yun, S., H. Zebker, P. Segall, A. Hooper, and M. Poland, 2007. Interferogram formation in the presence of complex and large deformation. *Geophysical Research Letters*, **34**: L12305.
- Zebker, H. and J. Villasenor, 1992. Decorrelation in interferometric radar echoes. *IEEE Transactions on Geoscience and Remote Sensing*, **30**: 950-959.
- Zebker, H.A., P.A. Rosen, S. Hensley, and P. Mouginis-Mark, 1996. Analysis of active lava flows on Kilauea volcano, Hawaii, using SIR-C radar correlation measurements. *Geology*, **24** (6): 495-498.
- Zebker, H. A., P. A. Rosen, and S. Hensley, 1997. Atmospheric effects in interferometric synthetic aperture radar surface deformation and topographic maps. *Journal of Geophysical Research*, **102** (B4): 7547-7563.